THEORETICAL STUDY OF THE EXCITON GROUND STATE IN SEMICONDUCTOR HETEROSTRUCTURES

The Fractional Dimension and the Variational Principle

RUTHBER ANTONIO ESCORCIA CABALLERO

UNIVERSIDAD INDUSTRIAL DE SANTANDER

FACULTAD DE CIENCIAS

ESCUELA DE FÍSICA

POSTGRADO EN FÍSICA MATERIA CONDENSADA

BUCARAMANGA

2004

THEORETICAL STUDY OF THE EXCITON GROUND STATE IN SEMICONDUCTOR HETEROSTRUCTURES

The Fractional Dimension and the Variational Principle

RUTHBER ANTONIO ESCORCIA CABALLERO

Submitted in partial fulfillment of the requirements for the degree of
Doctor of Physics

Director
ILIA D. MIKHAILOV Ph.D.

UNIVERSIDAD INDUSTRIAL DE SANTANDER

FACULTAD DE CIENCIAS

ESCUELA DE FÍSICA

POSTGRADO EN FÍSICA MATERIA CONDENSADA

BUCARAMANGA

2004

The undersigned hereby certify that they have read and recommend to the Faculty for acceptance a thesis entitled *"Theoretical study of the exciton ground state in semiconductor heterostructures: the fractional dimension and the variational principle"* in partial fulfillment of the requirements for the degree of Doctor of Physics

External Examiners: _____

_____

Research Supervisor: _____

Internal Examiner: _____

To my wife and my sons

ACKNOWLEDGMENTS

I want to thank the many people without whose help, support and friendship this thesis would not had been possible. In particular, I thank my supervisor Ilia Mikhailov for giving me the opportunity to pursue a PhD in his group and for his support and encouragement during the research. I also want to thank the Universidad del Magdalena for the permission to study at the UIS and its financial support as well.

My gratitude goes also to Francois Peeters for his guidance and support at University of Antwerp. Many thanks to Clara Riva for sharing work with me and all the friends in Belgium for helping to feel at home. I thanks also all my family and friends.

CONTENTS

	pág
INTRODUCTION	15
1. THEORETICAL BACKGROUND	19
1.1 BAND STRUCTURE OF SEMICONDUCTORS	19
1.2 THE EFFECTIVE MASS APPROXIMATION	22
1.3 EXCITONS	27
1.4 SEMICONDUCTOR HETEROSTRUCTURES	30
1.5 APPLICATIONS OF COMPOUND SEMICONDUCTORS	33
2. THE FRACTIONAL DIMENSIONAL APPROACH FOR EXCITONS IN HETEROSTRUCTURES	36
2.1 THEORETICAL MODEL	36
2.2 EXCITON IN FRACTIONAL DIMENSIONAL SPACE	39
2.3. THE CONFINEMENT POTENTIAL	44
3. APPLICTATIONS FOR A MODEL WITHOUT MAGNETIC FIELD	48
3.1 EXCITON IN SYMMETRICAL STEP QUANTUM WELLS	49
3.2 EXCITON IN CYLINDRICAL QUANTUM-WELL WIRES	54
3.3. EXCITON IN SPHERICAL QUANTUM DOTS	58
4. POLARONIC EXCITON IN QUANTUM-WELL WIRES AND NANOTUBES	63
4.1 INTRODUCTION	63

4.2 THEORETICAL MODEL 65

4.3 RESULTS AND DISCUSSION 68

5. HOLE MASS ANISOTROPY AND MAGNETIC FIELD EFFECTS 75

5.1 THEORETICAL MODEL 75

5.2 EXCITON IN QUANTUM WELLS AND QUANTUM WELL-WIRES 77

5.3 EXCITON IN TWO-DIMENSIONAL QUANTUM RING 80

6. CONCLUSIONS 91

REFERENCES 93

BIBLIOGRAPHY 98

FIGURES INDEX

pág.

Figure 1.1 Density of states for ideal crystal structures having different dimensions:
(a) three-dimensional or bulk, (b) two-dimensional or quantum well,
(c) one-dimensional or quantum wire and (d) zero-dimensional or quantum dot. 30

Figure 2.1 The radial part of the Jacobian (a) and running dimension
(b) dependences on the electron-hole separation in QW, cylindrical QWW and spherical QD. 42

Figure 2.2 Confinement potentials for a QW of width 200 Å modeled by using equation . 45

Figure 2.3 Different models of the confinement potential in a quantum wire of radius 400 Å. 46

Figure 3.1 Running dimension as a function of the electron-hole separation
for an exciton in a GaAs/$Ga_{0.7}Al_{0.3}As$ QW and for different well width. 50

Figure 3.2 Ground state binding energy of an exciton in a GaAs/$Ga_{0.7}Al_{0.3}As$ QW as a function
of the well width for different soft-edge barrier potentials. Solid circles correspond to theoretical
calculations from . 52

Figure 3.3 Exciton ground state binding energies as a function of the well width in a
GaAs/$Ga_{0.8}Al_{0.2}As$/$Ga_{0.55}Al_{0.45}As$ double-step QW and for several values of
the internal well width L_1 . 53

Figure 3.4 Ground state binding energy of an exciton in a GaAs/$Ga_{0.7}Al_{0.3}As$ QWW
as a function of the wire radius, for a model with rectangular potential (solid lines)
and soft-edge barrier (dashed and dotted lines). Solid circles (•) correspond to calculations. 56

Figure 3.5 Ground state binding energy of an exciton in a GaAs/$Ga_{0.8}Al_{0.2}As$/$Ga_{0.55}Al_{0.45}As$
coaxial QWW as a function of the wire radius, for a model with double-step quantum well potential. 58

Figure 3.6 Ground state binding energy of an exciton in a GaAs/$Ga_{0.7}Al_{0.3}As$ spherical QD

as a function of the dot radius for different soft-edge barrier potentials. 60

Figure 3.7 Ground state binding energy of an exciton in a GaAs/$Ga_{0.8}Al_{0.2}As$/$Ga_{0.55}Al_{0.45}As$ spherical QD as a function of the wire radius, for a model with double-step quantum well potential. 61

Figure 4.1 Exciton binding energies as a function of the well width for ZnSe/$Zn_{0.69}Cd_{0.31}Se$ (top) and GaAs/$Ga_{0.7}Al_{0.3}As$ (bottom) quantum wells. Solid curves correspond to values obtained by using the Aldrich and Bajaj V_{AB} potential for exciton-phonon interaction and dashed curves to those with Coulomb potential V_C. In the upper plot, a and b denote results as obtained with Luttinger parameters derived by Hölscher et al., and Sermage and Fishman [64 65] respectively. Open triangles correspond to theoretical calculations from Ref. [57] and solid triangles to experimental data from Ref. [61]. 70

Figure 4.2 Exciton binding energies as a function of wire radius for ZnSe/$Zn_{0.69}Cd_{0.31}Se$ (top) and GaAs/$Ga_{0.7}Al_{0.3}As$ (bottom) quantum wells wires. Solid curves correspond to values obtained by using the Aldrich and Bajaj V_{AB} potential for exciton-phonon interaction and dashed curves to those with Coulomb potential V_C. Open triangles correspond to theoretical calculations from Ref. [8]. 71

Figure 4.3 Binding energies for exciton in ZnSe/$Zn_{0.69}Cd_{0.31}Se$ quantum wires as a function of the heterostructure sizes and for different confinement potential shapes. Solid curves correspond to values obtained by using the Aldrich and Bajaj V_{AB} potential for exciton-phonon interaction and dotted curves to those with Coulomb potential V_C. 73

Figure 5.1 The light- and heavy-hole exciton binding energies as a function of the GaAs/$Ga_{0.7}Al_{0.3}As$ QW width. Open circles correspond to calculations from Ref. 6. 80

Figure 5.2 The light- and heavy-hole exciton binding energies as a function of the GaAs/$Ga_{0.7}Al_{0.3}As$ QW width for different magnetic field strengths. Open circles correspond to calculations from Ref. 7 81

Figure 5.3 Heavy-hole exciton binding energy as a function of the wire radius with and without magnetic field. Our results (solid lines) are compared with theoretical data from Ref. 8 (open circles). 82

Figure 5.4 Schematic representation of the electron conditional probability density in the x-z plane, for different QWW radii: (b) $R = 4.0a_0^*$, (c) $R = 1.0a_0^*$, (d) $R = 0.3a_0^*$

for the heavy-hole exciton with the fixed hole position at the wire axis. 83

Figure 5.5 Exciton binding energies in GaAs/$Ga_{0.7}Al_{0.3}As$ cylindrical QWWs with different confinement potential shapes as a function of the wire radius. 84

Figure 5.6 Exciton binding energy as a function of the ring width for different values of the magnetic field and core's radius. Inset in (a) shows the binding energy as a function of the magnetic field for a given ring width and in (b) shows the exciton binding energy in a quantum disk as a function of the disk radius. 88

Figure 5.7 Exciton binding energy as a function of the ring width, for three different profiles of the potential barriers. 89

INDEX TABLE

pág.

Table 1. Physical parameters for the GaAs/$Ga_{0.7}Al_{0.3}As$ and ZnSe/$Zn_{0.69}Cd_{0.31}Se$ heterostructures 69

THEORETICAL STUDY OF THE EXCITON GROUND STATE IN SEMICONDUCTOR HETEROSTRUCTURES

Author: Ruthber Antonio Escorcia Caballero*

A simple a general method for calculating the ground-state energy of an exciton in quantum confined structures in the presence of magnetic field and for different potential shapes is developed. In this method starting from the variational principle a one-dimensional wave equation, for the function that describe the intrinsic properties of the exciton and which depends only on the electron-hole separation, is obtained. The relation of this equation to the fractional dimensional approach is analyzed and it is shown that for a isotropic hole mass model, the equation describes a hydrogen-like atom in an effective isotropic space with non-integer dimension.

We investigate the influence of the magnetic field and the potential shape on the binding energies of excitons in quantum wells, quantum-well wires, quantum dots and quantum rings. We also study the effect of the longitudinal-optical phonon field on the exciton binding energies of exciton in heterostructures based on ionic semiconductors.

* Grade Work
** Science Faculty, Physics department, Ilia D. Mikhailov Ph.D.

ESTUDIO TEORICO DEL ESTADO BASE DEL EXCITON EN HETEROSTRUCTURAS SEMICONDUCTORAS

Autor: Ruthber Antonio Escorcia Caballero **

Un método general y simple para calcular la energía del estado base de un excitón en estructuras de confinamiento cuántico en la presencia de campo magnético y para diferentes formas del potencial es desarrollado. En este método se parte del principio variacional y se deriva una ecuación de onda unidimensional para la función que describe las propiedades intrínsecas del excitón, la cual depende únicamente de la separación electrón-hueco. La relación de esta ecuación con el método de dimensionalidad fraccionaria es analizada y se muestra que para el caso del modelo isotrópico para el hueco en el excitón, esta ecuación describe un átomo hidrogenoide en un espacio isotrópico efectivo con dimensión no entera.

La influencia del campo magnético y la forma del potencial de confinamiento sobre la energía de enlace del excitón en pozos cuánticos, hilos de pozo cuántico, puntos cuánticos y anillos cuánticos es investigada. También se estudia el efecto del campo fonónico óptico longitudinal sobre la energía de enlace del excitón en heterostructuras basadas en semiconductores iónicos.

---

[*] Trabajo de grado

[**] Facultad de Ciencias, Escuela de Física, Dr. Ilia D. Mikhailov

INTRODUCTION

Semiconductor heterostructures is one of the most important subjects in modern solid-state physics. In 2000, Alferov and Kroemer shared the Nobel prize in Physics "for developing semiconductor heterostructures used in high-speed- and opto-electronics", with Killby "for his part in the invention of the integrated circuit". By combining two semiconductor materials with different bandgaps, it is possible to manufacture a heterostructure to have a desired band offset. This the basis of what is called *bandgap engineering*. Development of the physics and technology of semiconductor heterostructures has resulted in remarkable achievements, among others, the fabrication of quantum well lasers, and recently quantum dot lasers. Currently, most double heterostructure laser are based on quantum well structures, where the motion of carriers is restricted to two directions [1]. However, as the physics and applications of these quantum well structures rapidly progressed, scientists were drawn to the study of structures with further reduced dimensionality, namely quantum wires and dots, which exhibit quantum confinement of charge carrier in respectively two and three directions.

The progress in nanoscale technology has made possible the fabrication of low-dimensional heterostructures with controlled thickness and relatively sharp interfaces, where the excitons remain present even at room temperature because of the quantum confinement increases highly the electron-hole attraction [1-4]. Excitons in semiconductor nanostructures have a larger binding energy and oscillator strength with respect to their

bulk values. This gives rise to a rich variety of enhanced optical properties which are of considerable relevance for potential applications in novel electronic and optoelectronic devices [3]. A great deal of attention has been devoted to experimental and theoretical studies of excitons in heterostructures based on III-V semiconductor particularly quantum wells (QWs), superlattices (SLs), quantum-well wires (QWWs), quantum dots (QDs) and more recently quantum rings (QRs) [5-24]. Different phenomena have also been included in these calculations such as effective-mass and dielectric constant mismatch between the well and the barrier materials [15], valence-band mixing and non-parabolicity of the dispersion relations [13], but only few papers concerned with effect of the confining potential shape on the exciton energy have been reported. Up to now it has been considered the confinement models with square-well [5, 13], parabolic [10] and charge image [11] potentials.

The main difficulty to analyze the spectrum of exciton in quantum confined systems is related to the fact that the Hamiltonian cannot be separated into center-of-mass and relative-motion terms except in the case of isotropic parabolic confinement as the electron and the hole effective masses are equals. In other cases, approximation methods such as the variational [8, 9], matrix diagonalization [10], finite element [14], stochastic variational [18] and finite difference [19] have to be used. In spite of the fact that these techniques give consistent results with experimental data, in most of the cases they entails a lot of computational work and the accuracy of the variational method depends to a large extent on the form of the trial wave function.

In the last decade, it has been proposed an alternative mathematical approach that allows us to treat anisotropic interactions in a three-dimensional space as isotropic ones in a lower fractional-dimensional space, where the dimension is determined by the degree of anisotropy. This approach was first applied by He [25], who using the hydrogen-like Hamiltonian in an effective fractional space proposed by Stillinger [26] treated the interband optical transitions and bound excitons in strongly anisotropic semiconductors. Lefebvre and co-investigators [27] applied this method to analyze the exciton energy states and the absorption spectra in QWs and QWWs. They considered the fractional dimension as a phenomenological parameter related to the heterostructure geometry and proposed a simple exponential-law dependence of this parameter on the average electron-hole distance in the unbound state. A different method to determine the appropriate fractional dimensionality, in GaAs-(Ga, Al)As QWs, QWWs, QDs and superlattices (SLs) by fitting the ground state energy of the isotropic hydrogenic-like model in fractional-dimensional space to the actual three-dimensional system has been proposed recently by Oliveira and co-investigators [28]. In spite of the fact that this approach makes the calculation of the exciton binding energy free of tedious computation, it breaks down in the case of strong confinement, for example, in QWWs and QDs of very small sizes, or for strong magnetic fields.

Recently, we have proposed a simple variational procedure related to the fractional-dimensional approach in which the wave equation for a donor impurity D^0 in quantum well heterostructures is reduced to one similar to that for hydrogenic atom in an isotropic effective space with fractional dimension [29-30]. It has been established that this procedure provides an efficient algorithm for calculating the ground state binding energies

with accuracy comparable with those of sophisticated methods such as the series expansion and Monte Carlo [30].

In this thesis we develop an unified method to study the ground state of an exciton in different semiconductor heterostructures in the presence of magnetic field, taking into account the anisotropy of the hole effective mass and considering different confining potential shapes. In the second chapter the general theory for excitons in semiconductor heterostructures is presented. In the third chapter the method is applied to the study of exciton ground state in graded quantum-well heterostructures (QWs, QWWs, QDs) without an applied magnetic field. The fourth chapter is devoted to the study of the effect of the longitudinal-optical phonon field on the binding energy of excitons in QWs, QWWs and nanotubes based on ionic semiconductors. In the fifth chapter the method is developed for a system that takes into account the anisotropy of hole mass for excitons in QWs, QWWs and QRs in the presence of magnetic field. Finally the conclusions are presented.

1. THEORETICAL BACKGROUND

1.1 BAND STRUCTURE OF SEMICONDUCTORS

A crystal is a periodic array of atoms which can be describe through a Bravais lattice with a basis [31]. The periodical position of the atoms is due to the nature of the bonding. In the binding process neighboring atoms share only a few outer electrons, while their cores remain on the sites that define the periodical lattice. If we neglect the impurities in the crystal (ideal crystal) and we consider the cores fixed at their lattice sites (adiabatic approximation), those shared electrons feel a periodic potential generated from the ionic cores in the underlying lattice. Thus, the Hamiltonian of a single outer-shell electron in the lattice is

$$H = -\frac{\hbar^2}{2m_e}\nabla^2 + U(\mathbf{r}), \tag{1.1}$$

where m_e is the mass of the electron and $U(\mathbf{r})$ is the periodic potential with periodicity equal to the lattice constant. The Bloch theorem tells us that the solution of the Schrödinger equation associated to the Hamiltonian (1.1) can be written in the form

$$\Phi_{n\mathbf{k}}(\mathbf{r}) = e^{i\mathbf{k}\cdot\mathbf{r}} u_{n\mathbf{k}}(\mathbf{r}), \tag{1.2}$$

where $u_{n\mathbf{k}}(\mathbf{r})$ has the same periodicity of the lattice and $\mathbf{k}$ has the dimension of a momentum, in units of $\hbar = 1$, and is known as crystal momentum. The vector $\mathbf{k}$ is related

to the translational invariance of the system and in particular is the corresponding of the vector $\mathbf{r}$ in the reciprocal lattice, i.e. the lattice which is built from the original one in such a way that if the lattice constant of the Bravais lattice in the space is a, the lattice constant of the reciprocal lattice is π/a.

For each value of $\mathbf{k}$ we obtain a set of eigenvalues $E_n(\mathbf{k})$ which constitutes the electronic spectrum for an electron with a given momentum $\mathbf{k}$. When we vary n and $\mathbf{k}$, a discrete series of continuum intervals of allowed values for the energy of the electron is described. These intervals are normally referred to as electronic bands for the crystal and represented with $\mathbf{k}$ in the first Brillouin zone. Thus, using only the translational invariance of the crystal lattice, one can derive the band structure of the system. Even though this is a simplified picture and many properties of the band structure cannot be explained in this simplified way, it serves well the scope of giving an idea of the concept of band structure of a crystal. A more precise and detailed explanation can be found in many review papers and books [32]. The calculation of the exact band structure is, still today, a subject of research and refinement.

The electrons in a crystal fill the electronic bands starting from the lowest one and at $T = 0$ the highest occupied band is either completely or partially filled. When the bands are completely filled, no current can be transported, i.e. the material is an *insulator*, when one of the band is partially filled, there is the possibility of current transport, i.e. the material is a metal. The difference between the minimum of the first empty band and the maximum of the highest filled band is referred to as energy band gap, i.e. gap, and is the minimum

quantum of energy required to trigger an interband transition. When the temperature is non zero, the electrons can move from the highest filled band to the first empty band with a probability given by $\exp\left(-E_g/T\right)$, where E_g is the energy gap and T the absolute temperature. Thus if the energy gap is small enough some electrons will jump for a finite temperature to the first empty band and the material will become conducting. In this case we will say that the material is a *semiconductor*. The energy band gap, E_g, of a semiconductor is typically of the order of $1eV$, e.g. E_g is equal to $1.42eV$ for GaAs at $T = 300K$.

In III-V binary compounds like GaAs, there are 8 outer electron per unit cell which contribute to the chemical bonds. The other electrons of each kind of atom are "frozen" in closed shell configurations and their wave functions are highly bound around the Ga or As nuclei. They do not contribute to the electronic properties. The 8 outermost electrons hybridize to form tetrahedral bonds between one kind of atom (e.g. Ga) and its nearest neighbors (As). The orbitals of every atom (s-like or p-like) hybridize with an orbital of the neighboring atom, thus producing two levels: one bonding and one antibonding. Because of the large number of unit cells, bonding and antibonding levels broaden into bands [33]. The bonding levels are completely filled with electrons, an form the *valence* bands while the empty (antibonding) ones form the *conduction* bands. Thus, the completely filled band at $T = 0$ is called the valence band while the first empty band is called the conduction band.

In all III-V materials the top of the valence band occurs at the center of the Brillouin zone (the Γ point). In the absence of spin-orbit coupling, the three valence bands (which

originate from the bonding p orbitals) are degenerate at Γ. The spin-orbit coupling lifts this sixfold degeneracy and gives rise to a quadruplet and a doublet in the following way. Since the valence band is built from *p*-type orbitals, its states carry and internal (band) angular momentum L equal to unity. In a system with circular symmetry (e.g. bulk semiconductor, quantum well, circular quantum dot) both the total angular momentum length J and its projection along the axis of symmetry J_z are good quantum numbers of a single, non-interacting particle. Denoting the spin angular momentum $\boldsymbol{\sigma}$ and the internal (band) angular momentum $\mathbf{L}$, we have $\mathbf{J} = \boldsymbol{\sigma} + \mathbf{L}$. The single particle states of the valence band are then classified in the following way, according to the values of $(J, J_z) = (|\boldsymbol{\sigma} + \mathbf{L}|, \boldsymbol{\sigma}_z + \mathbf{L}_z)$: $(3/2, \pm 3/2)$, heavy-hole subband, $(3/2, \pm 1/2)$, light-hole subband, $(1/2, \pm 1/2)$, split-off subband, where the quadruplet $J = 3/2$ is in III-V compounds always higher in energy than the doublet $J = 1/2$. Their energy separation is denoted Δ and called the spin-orbit splitting. The conduction band is built from *s*-type orbitals and therefore has $L = 0$. Addition to $\sigma = 1/2$ only gives $J = 1/2$ (doublet).

1.2 THE EFFECTIVE MASS APPROXIMATION

In general the study of the properties of a crystal requires the study of the collective motion of the arrays of atoms, i.e. nuclei and electrons, forming the crystal itself. However, if one is allowed to consider only an electron with momentum $\mathbf{k}$ in the vicinity of a critical point labeled $\mathbf{k}_c$, its energy $E(\mathbf{k})$ can be written using a Taylor series expansion around $\mathbf{k}_c$,

$$E(\mathbf{k}) = E(\mathbf{k}_c) + \sum_{i,j}^{3} \frac{\partial^2 E}{\partial k_i \partial k_j}(\mathbf{k})\Big|_{\mathbf{k}=\mathbf{k}_c} (k_i - k_{ci})(k_j - k_{cj}), \tag{1.3}$$

where $\partial^2 E(\mathbf{k}) / \partial k_i \partial k_j \big|_{\mathbf{k}=\mathbf{k}_c}$ is a tensor that does not depend on $\mathbf{k}$. This tensor can be used in order to define a "new" mass of the electron called *effective mass of the electron*, m_e^*, such as

$$\frac{\partial^2 E}{\partial k_i \partial k_j}(\mathbf{k})\Big|_{\mathbf{k}=\mathbf{k}_c} = \frac{\hbar^2}{2m_e^*(\mathbf{k})_{ij}}\Big|_{\mathbf{k}=\mathbf{k}_c} . \tag{1.4.}$$

If we substitute Eq. (1.4) in Eq. (1.3) we obtain

$$E(\mathbf{k}) = E(\mathbf{k}_c) + \sum_{i,j}^{3} \frac{\hbar^2}{2m_e^*(\mathbf{k})_{ij}}\Big|_{\mathbf{k}=\mathbf{k}_c} (k_i - k_{ci})(k_j - k_{cj}), \tag{1.5}$$

this expression is very similar to the one of a free electron with a renormalized mass. In particular if we choose a particular direction, i.e. $\hat{a}$, we obtain

$$E(\mathbf{k} \cdot a) = E(\mathbf{k}_c) + \frac{\hbar^2}{2m_{ea}^*} k_a^2, \tag{1.6}$$

where m_{ea}^* is the effective mass of the electron along the direction $\hat{a}$. We can then say that the net effect of the crystal potential on the electron inside the crystal is to change the electron mass form the value in free space to the effective mass m_e^*. Thus the effect of the periodic potential crystal potential is accounted for by the effective mass itself.

In particular for GaAs, the material of central interest in this thesis, an expansion of the conduction band about the minimum energy is approximately parabolic [34], due to the *s*-type symmetry of the minimum at the Γ point. This define an effective mass which is independent from the direction. For the valence band the situation is more complicated due

to its symmetry at the Γ point. Indeed following Dresselhaus [35] the band structure at the Γ point can be written as

$$E(k) = E(k_{\Gamma v}) \pm \left[Bk^4 + C\left(k_x k_y + k_y k_z + k_x k_z\right) \right]^{1/2}, \tag{1.7}$$

where $k_{\Gamma v}$ is the value of k for which the valence band has a maximum $k - k_{\Gamma v} = (k_x, k_y, k_z)$ and B, C are constants. Notice that the value of the effective mass will, in this case, not only depend on the direction along which it is calculated, but also on which of the two degenerate band the particle belongs to. However, spherical approximations for the effective mass are available also for the valence band. In the particular case of the holes, the will be called light-hole (if $+$ is chosen in Eq. 1.7), heavy-hole (if $-$ is chosen in Eq. 1.7), depending on which band originates them. In particular, as the effective mass is inversely proportional to the curvature of the band in the point, the band with the smallest curvature generates the heavy-hole.

The motion of a conduction band electron in the presence of an external potential $V(\mathbf{r})$ can be described in the effective mass approximation by the Hamiltonian

$$H = \frac{\mathbf{p}^2}{2m_e^*} + V(\mathbf{r}), \tag{1.8}$$

where m_e^* is the effective mass, $\mathbf{r}$ is the position vector and $\mathbf{p}$ is the momentum. In the simplest approach, all hole subbands are treated independently. Each subband is characterized by a pair of effective masses $m_{h\perp}^*$ and $m_{h\square}^*$, defining respectively the dynamics in plane and along the axis of symmetry. The Hamiltonian for a hole in the presence of an external potential in the effective mass approximation can thus be written as

$$H = \frac{p_{\square}^2}{2m_{h\square}^*} + \frac{\mathbf{p}_{\perp}^2}{2m_{h\perp}^*} + V(\mathbf{r}), \tag{1.9}$$

where the masses $m_{h\perp}^*$ and $m_{h\square}^*$ will be different whether the heavy hole or the light hole is considered.

A more accurate description of holes, however, requires taking into account the interaction between the subbands (intersubband mixing). The so-called $\mathbf{k}\cdot\mathbf{p}$ theory meets this requirement. In a bulk crystal, the one-electron Schrödinger equation which has to be solved is:

$$\left[\frac{\mathbf{p}^2}{2m_0} + V(\mathbf{r}) + \frac{\hbar^2}{4m_0^2c^2}(\boldsymbol{\sigma}\times\nabla V).\mathbf{p}\right]\Psi(\mathbf{r}) = E\Psi(\mathbf{r}), \tag{1.10}$$

where m_0 is the free electron mass, $V(\mathbf{r})$ is the effective lattice potential caused by the ions and core electrons, and the third term in the spin-orbit coupling (σ is the electron spin) [36]. The Bloch theorem states that the wave function in a crystal can be written as the product $\Psi_{n\mathbf{k}}(\mathbf{r}) = e^{i\mathbf{k}\cdot\mathbf{r}}u_{n\mathbf{k}}(\mathbf{r})$, where $u_{n\mathbf{k}}(\mathbf{r})$ is the atomic lattice periodic part of the total wave function, n is the band index and $\mathbf{k}$ lies within the first Brillouin zone. The periodic parts of the Bloch function, $u_{n\mathbf{k}}(\mathbf{r})$, are then solutions of

$$\left\{\frac{\mathbf{p}^2}{2m_0} + V(\mathbf{r}) + \frac{\hbar}{4m_0^2c^2}(\boldsymbol{\sigma}\times\nabla V).\mathbf{p} + \frac{\hbar^2k^2}{2m_0} + \frac{\hbar\mathbf{k}}{m_0}\cdot\left[\mathbf{p} + \frac{\hbar}{4m_0c^2}(\boldsymbol{\sigma}\times\nabla V)\right]\right\}u_{n\mathbf{k}}(\mathbf{r}) = E_{n\mathbf{k}}u_{n\mathbf{k}}(\mathbf{r}). \tag{1.11}$$

Note the operator $\mathbf{k}\cdot\mathbf{p}$ in this expression, which gives the method its name ($\mathbf{k}\cdot\mathbf{p}$ Method). To deal with Eq. (1.10), the equation for $\mathbf{k} = \mathbf{0}$ has to be solved, giving the eigenfunction

u_{n0} and eigenenergies E_{n0}. An arbitrary lattice periodic function can then be written as a series expansion using the eigenfunctions u_{n0},

$$u_{n\mathbf{k}} = \sum_m c_m^n(\mathbf{k}) u_{m0}, \tag{1.12}$$

where the summation runs over all bands. Inserting this in Eq. (1.10) and solving the resulting matrix equation will give the exact eigenstates of our wave equation. However, such a calculation becomes increasingly complicated as $\mathbf{k}$ increases. A possible way to handle this is to treat the terms in $\mathbf{k}$ as perturbations. Since the perturbation terms will be proportional to k, the method works best for small values of k. The second order eigenenergies can then be written as

$$E_{n\mathbf{k}} = E_{n0} + \frac{\hbar^2 k^2}{2m_0} + \frac{\hbar^2}{m_0^2} \sum_{m \neq n} \frac{\left| \left\langle u_{n0} \left| \mathbf{k} \cdot \left[\mathbf{p} + \frac{\hbar}{4m_0 c^2} (\boldsymbol{\sigma} \times \nabla V) \right] \right| u_{m0} \right\rangle \right|^2}{E_{n0} - E_{m0}}, \tag{1.13}$$

which, for small values of k, is generally written as

$$E_{n\mathbf{k}} = E_{n0} + \frac{\hbar^2 k^2}{2m^*}, \tag{1.14}$$

where m^* is defined as the effective mass of the band. This approach works well when the energy difference between the considered bands, $E_{n0} - E_{m0}$ is large.

However, especially for the complicated valence band, a more exact approach including the strong band to band interaction, is required. This can be done by treating *exactly* only those bands that are strongly coupled and correcting this approximation by treating the influence of the energetically more distant bands perturbatively. This approach is called "Kane's model" [37]. As there are 8 bands treated exactly (the lowest conduction band, and the

heavy-hole, light-hole and split-off valence band, all doubly degenerate due to spin), it is often also referred to as 8×8 or 8-band $\mathbf{k}\cdot\mathbf{p}$ theory. The inclusion of 8 bands gives a Hamiltonian which is an 8×8 matrix equation. An alternative approach was developed by Luttinger and Kohn [38]. In zinc-blende type semiconductors, it is not unrealistic to assume that both the energy gap E_g and the spin-orbit splitting Δ are large. Typical values are $E_g = 1.520\,eV$ and $\Delta = 0.341\,eV$ for GaAs, $E_g = 0.420\,eV$ and $\Delta = 0.38\,eV$ for InAs, $E_g = 1.424\,eV$ and $\Delta = 0.110\,eV$ for InP. Therefore it will be enough to treat exactly only the heavy- and light-hole valences bands and to consider both the conduction and split-off bands as distant, thus including them in the perturbation. The Hamiltonian equation will then be reduced to a 4×4 matrix equation.

1.3 EXCITONS

It is known that in a ideal case and at low temperature all the electrons in the crystal sit in the "valence band". The question is what will happen if we excite one of those valence electrons?. The electron will jump to the conduction band, if the energy of the excitation is larger or equal to the energy band gap. It is, however, wrong to think that if the energy of the excitation is smaller than the energy gap there will be no transition at all. For example, the absorption spectra observed for a bulk GaAs sample near the band gap at different temperatures show that the absorption coefficient does not increase continuously for energies larger than the gap energy gap, as it would be expected if the electron could only

be promoted to the conduction band, but presents a peak below the energy band gap which suggests the presence of discrete states in the gap.

It must be noticed that the conduction band is not built considering the allowed energy values for the excited states of a N electrons system, but it is built considering the allowed energy values for the $N+1$ electron in a system with $N+1$ electrons. From the correct treatment of the N particles problem a new state in the gap arises, i.e. the excitonic state. This can be described as the bound state of an electron in the conduction band interacting with a positive charge in the valence band, i.e. a hole, and it can be shown that this states lies in the gap. In fact, the conduction electron is attracted, through the Coulomb interaction, to the positively charged hole left behind in the valence band. As a result, the electron and hole form the bound state called an *exciton*. Because of the attractive Coulomb energy, the energy of the exciton will be lower compared to the energies of a free electron and hole. The difference is called the exciton binding energy. The exciton levels are therefore found in the band gap region of the semiconductor. When the electron falls back into the valence band, i.e. electron and hole recombine, a photon is emitted. This process, known as luminescence, is the reverse process to absorption. The experimental technique measuring the energy of this emitted photon is called photoluminescence spectroscopy.

In most semiconductors, the Coulomb interaction is strongly screened by the valence band via the large dielectric constant. As a result, electrons and holes are only weakly bound. Such excitons are known as *Wannier-Mott excitons* or simply as *Wannier excitons*. Its properties can be calculated with the effective mass approximation. Within this

approximation, the electron and the hole are considered as two particles moving with effective masses of the conduction and valence bands respectively. Donors and acceptors can be regarded as "excitons" in which one of the particles has an infinite mass. Since the difference in effective mass between the electron and the hole in a semiconductor is not as large as that between the electron and the proton, excitons are more analogous to *positronium*, an electron-positron par. As a result of the Coulomb interaction between the electron and hole, the potential acting on an electron (or a hole) in a crystal is not translationally invariant. As any two-particle system, the exciton motion can be decomposed into two parts: a *center-of-mass* (CM) *motion* and a *relative motion* of the two particles about the CM. With this decomposition , the potential acting on the exciton CM still has translational invariance since the Coulomb interaction depends only on the *relative coordinate* of the electron and hole. Within the effective mass approximation, the exciton CM behaves like a free particle with mass $M = m_e^* + m_h^*$. The relative motion of the electron and the hole in the exciton is similar to that of the electron and the proton inside the hydrogen atom. There are bound states and continuum states. The bound states are quantized with principal quantum number $n = 1, 2, 3$, etc., and orbital angular momentum $l = 0, \hbar, 2\hbar$, etc. In the continuum states, excitons can be considered to be ionized into free electrons and free holes but their wavefunctions are still modified by their Coulomb interaction.

1.4 SEMICONDUCTOR HETEROSTRUCTURES

The ions in a perfect three-dimensional (3D) bulk crystal are arranged in a regular periodic array and thus the electronic structure can be considered as an electron in the presence of a potential with the periodicity of the underlying Bravais lattice. This leads to a description of the electron energy levels as a set of continuous functions having the periodicity of the reciprocal lattice [31]. For semiconductors, this results in the existence of an energy bandgap, E_g, between the valence and the conduction bands. Much experimental and theoretical work [31-33] has been done to obtain detailed band structures of various semiconductor elements and their compounds. It can be shown [39, 40] that the number of available electron states per volume, i.e. the density of states $n(E)$, is zero for the lowest-energy state in a 3D crystal and that $n(E)$ increases as the square root of the energy, as shown in Fig. 1.1 (a).

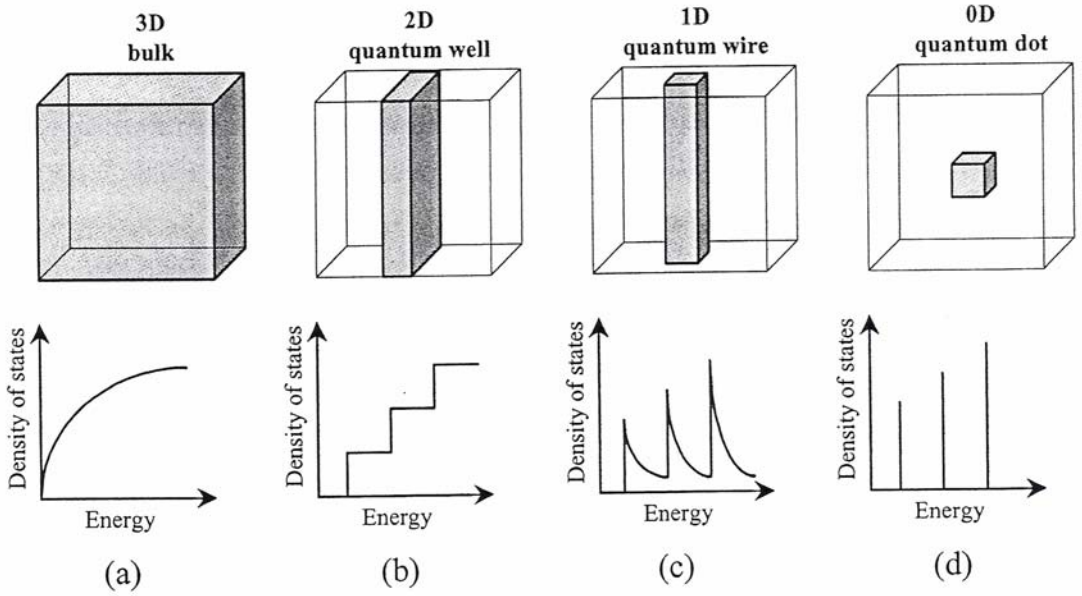

Figure 1.1 Density of states for ideal crystal structures having different dimensions: (a) three-dimensional or bulk, (b) two-dimensional or quantum well, (c) one-dimensional or quantum wire and (d) zero-dimensional or quantum dot.

When the dimensionality is reduced to a two-dimensional (2D) crystal, the electronic structure of the free charges is highly influenced. For example, $n(E)$ is changed from a continuous to step-like function, as presented in Fig. 1.1 (b). Such a 2D crystal can be realized using modern epitaxial techniques by growing, for example, a thin GaAs film between two films of the larger bandgap semiconductor $Ga_{1-x}Al_xAs$. The finite conduction and valence-band offsets of the two semiconductors produce potential barriers for the electrons in the conduction band and holes in the valence band, and when GaAs thickness is of the order of the electron de Broglie wavelength, the motion of the charges is restricted to a 2D plane which is therefore called a quantum well (QW). The particles can move as free waves in the plane of the well while in the other direction, perpendicular to the QW, their motion is restricted by the potential barriers. For typical semiconductors, the well with is of the order of nanometers. These systems are of crucial importance for practical devices. For example, in lasers manufactured from bulk materials, the excitation process excites many electrons to a higher energy level but only few of them have the exact energy to take part in the stimulated emission process. For 2D systems, the nature of $n(E)$ allows a non-zero number of electrons to occupy the lowest-energy state so that more electrons can participate in stimulated emission. This results in a reduced laser current density and higher lasing-efficiency [41].

A further reduction of the dimensionality to one-dimensional structure (1D) leads to a quantum wire (QWR). This can be realized, for example, by growing a second QW perpendicular to a cleaved QW so that the intersection of both QWs results in a 1D

structure. Other techniques as electron beam lithography in combination with etching [42] or self-organization [43] can be used to manufactured QWRs. The density of states of a 1D structure consists of sharp peaks with a tail on the high-energy side as presented in Fig. 1.1 (c). Theoretically, the lasing threshold current density is expected to be much lower in the 1D case but practical problems in growing large numbers of high-quality QWRs hampers their realization [44].

The ultimate charge confinement, leading to charge localization in all three dimensions occurs in a zero-dimensional (0D) structure or quantum dot (QD). The 3D band structure completely disappears and a discrete δ-function like energy levels arise with an energy difference depending on the size of the QD (see Fig. 1.1 (d)) QD structures are therefore often called "artificial atoms" [45]. All the electrons in the ground state have the same energy which results in a threshold current density of QD laser about 100 times lower than for QW lasers [1]. Research on QDs using a variety of manufacturing techniques is widely extended and reveals new insights into the physics of charge confinement. A variety of quantum dot structures exists, but most promising for device applications are the so-called self-assembled quantum dots, as their growth process is easily realizable, rather fast and not too expensive: they form spontaneously during the growth of strained heterostructures, i.e. they literally "self-assemble". QDs can also be used to make devices with a totally new functionality, such as *quantum dot based memory devices*, where the information is stored as a single or few electrons. It is predicted that these memory devices could potentially achieve ultra-dense storage capacities. Thanks to the self-organization process for QDs is has also been possible the fabrication of novel confined structures called quantum rings (QRs), which possess unique features, for instance, the observation of the Aharonov-Bohm

effect [22]. The same procedure is used as the formation of QDs, the only step necessary to induce the transformation form dots to rings, is introducing a short growth interruption during the process allowing the material extra time to rearrange itself.

1.5 APPLICATIONS OF COMPOUND SEMICONDUCTORS

The majority of important semiconducting materials are isoelectronic with elemental silicon. In silicon each atom provides 4 valence electrons one to each of 4 neighbors, which leads to a filled valence band. Other important materials are III-V materials, e.g., GaAs, InP or II-VI materials as CdS or ZnSe. These compound semiconductors are formed by combining elements displaced on either side of silicon by one place (III-V) or two places (II-VI) in the periodic table. One important feature of compound semiconductors is that many of these materials have band gaps which are in useful regions of the electromagnetic spectrum. In particular we can identify the visible region for use in energy conversion (solar cells) and display technologies and the infrared region for thermal imaging technologies [46].

The applications of III-V materials represent a fairly well developed area of technology. The majority of the applications of such semiconductors are in the area of opto-electronics and there are many commercial processes for the manufacture of light emitting diodes (LEDs) or solid state lasers. Gallium arsenide solar cells are commonly used in the solar panels used to power satellites. There is a current interest in developing LED and laser technologies for the blue end of the electromagnetic spectrum as all of the present mayor

technologies produce red lasers; gallium nitride is a promising material in this context. The majority of III-V semiconductors are direct band gap materials which makes them especially effective in opto-electronic applications. However, because electrons can be accelerated to a higher velocity in GaAs than in Si, there is also the potential to produce faster electronic devices in GaAs than those fabricated in silicon. Some effort has been expended towards developing GaAs technologies but the dominance of silicon in the mainstream electronic industry probably means that silicon technology will dominate conventional electronic devices for the foreseeable future. However, II-V technology is a mature and important area of the electronics industry as can be judged from the following examples. The methods of fabrication of III-V devices range from liquid phase epitaxy to vapor phase techniques such as MOCVD, It is probably a useful simplification to suggest that cheap mass produced products such as LEDs are currently manufactured by LPE whereas high value added devices such as solid state laser for major fiber optical links are produced by more expensive methods such as MOCVD which allow for greater control of morphology, doping and structure.

The II-VI compounds are generally direct band gap semiconductors like the III-V compounds that form the basis of mot opto-electronic devices at present, but the band gap energies of II-VI materials are larger than those of II-V materials. These characteristics mean that II-VI semiconductors are potentially important materials for the emission, detection, and modulation of light in the visible and near-UV region [46]. In contrast the III-V compounds are suitable for the visible (largely red) to near-IR radiation. Due to inherent disadvantages in II VI compounds, its application has generally been limited to simple applications as in optical coatings, gratings or photoconductors. However, hetero-

epitaxial technologies have now started to be developed and recent advances in MOCVD may open up new device applications. ZnS and ZnSe are the most promising materials for blue/blue-green laser diode devices which could lead to a high density optical storage systems, as well as fast switching devices. Of all the growth techniques employed for thin layers of II-VI materials only MBE has, as yet, led to successful doping. In 1991, both *p*- and *n*-type doping became controllable in a MBE system and a blue emitting laser diode with a single quantum well (SQW) structured based on the ZnSe *p*-*n* junction was fabricated. More recently and advanced multi-quantum well structure leading to CW emission even at room temperature has been reported [46].

2. THE FRACTIONAL DIMENSIONAL APPROACH FOR EXCITONS IN HETEROSTRUCTURES

2.1 THEORETICAL MODEL

In this part of the thesis we consider a single exciton in semiconductor heterostructures within the effective mass approximation by using an spherical hole mass approximation and constant physical parameters throughout the heterostructures [8]. In this case the characteristic energy of an exciton can consequently be defined through the effective Rydberg $R_y^* = e^2/2\varepsilon a_0^*$, and its characteristic length through the effective Bohr radius, $\mathrm{a}_\mathrm{o}^* = \varepsilon\hbar^2/\mu e^2$, with $\mu = m_e^* m_h^*/\left(m_e^* + m_h^*\right)$ being the reduced exciton effective mass. Thus the dimensionless Hamiltonian for the electron-hole pair confined in a heterostructure in the presence of an external field may be written as:

$$H\left(\mathbf{r}_e, \mathbf{r}_h, \tau\right) = H_e\left(\mathbf{r}_e\right) + H_h\left(\mathbf{r}_h\right) + V_{ext}\left(\mathbf{r}_e, \mathbf{r}_h\right) - 2\tau/r_{eh} \quad (\tau = 0,1), \tag{2.1}$$

$$H_e = -\eta_e \nabla_e^2 + V_e\left(\mathbf{r}_e\right); \qquad H_h = -\eta_h \nabla_h^2 + V_h\left(\mathbf{r}_h\right), \tag{2.2.}$$

where H_e and H_h describe the free motion of electron and hole confined in the heterostructure respectively, $V_{ext}\left(\mathbf{r}_e, \mathbf{r}_h\right)$ is a perturbation due to the presence of the external field, $-2/r_{eh}$ is the energy of the electron-hole interaction , $\mathbf{r}_e$ and $\mathbf{r}_h$ are electron and hole position vectors, and $r_{eh} = \left|\mathbf{r}_e - \mathbf{r}_h\right|$ is the electron-hole separation. The parameter τ in Eq.(2.1) is equal to 1 for exciton and to 0 for uncorrelated electron-hole pair, and the

parameters $\eta_e = \mu/m_e^*$ and $\eta_h = \mu/m_h^*$ in Eq.(2.2) are characteristics of the corresponding dimensionless effective masses of the hole in units of the reduced exciton effective mass μ respectively.

For an uncoupled electron-hole pair ($\tau = 0$), the Hamiltonian (2.1) is separable and the solution of the Schrödinger equation for the ground state of this system can be easily found by solving the eigenvalue problem

$$H(\mathbf{r}_e, \mathbf{r}_h, \tau = 0) f_0(\mathbf{r}_e, \mathbf{r}_h) = E_0 f_0(\mathbf{r}_e, \mathbf{r}_h). \tag{2.3}$$

On the contrary for exciton ($\tau = 1$), the Schrödinger equation

$$H(\mathbf{r}_e, \mathbf{r}_h, \tau = 1)\Psi(\mathbf{r}_e, \mathbf{r}_h) = E_{ex}\Psi(\mathbf{r}_e, \mathbf{r}_h), \tag{2.4}$$

can only be solved by using some approximation methods. Assuming that the center of mass motion is affected by the electron-hole interaction to a considerably smaller degree than the relative motion, we choose the ground state exciton trial function in the form:

$$\Psi(\mathbf{r}_e, \mathbf{r}_h) = f_0(\mathbf{r}_e, \mathbf{r}_h)\Phi(r_{eh});\ r_{eh} = \sqrt{(x_e - x_h)^2 + (y_e - y_h)^2 + (z_e - z_h)^2}, \tag{2.5}$$

where $f_0(\mathbf{r}_e, \mathbf{r}_h)$ is the product of the one-particle electron and hole ground state wave functions, whereas $\Phi(r_{eh})$ is a variational function that describes the intrinsic properties of the exciton and depends only on the electron-hole separation. The ground state energy of the exciton is found by minimizing the following functional

$$F[\Phi] = \int d\mathbf{r}_e d\mathbf{r}_h f_0 \Phi [H - E_{ex}] f_0 \Phi. \tag{2.6}$$

As explained in Ref. [30] after some algebraic manipulations we can obtain the following variational problem:

$$F[\Phi]=\int_0^{\infty}\left\{J_0(r)\left[\left(\frac{d\Phi(r)}{dr}\right)^2+\left(E_0-E_{ex}-\frac{2}{r}\right)\right]\Phi^2(r)\right\}dr\rightarrow\min, \tag{2.7}$$

with $E_0=E_e+E_h$ being the ground state energy of the uncoupled electron-hole pair, $r=r_{eh}$ and

$$J_0(r)=\int d\mathbf{r}_e\int f_0^2(\mathbf{r}_e,\mathbf{r}_h)\,\delta\left(|\mathbf{r}_e-\mathbf{r}_h|-r\right)d\mathbf{r}_h. \tag{2.8}$$

The minimization of the functional (2.7) with respect to Φ and its first derivative yields the Euler-Lagrange equation

$$-\frac{1}{J_0(r)}\frac{d}{dr}J_0(r)\frac{d\Phi(r)}{dr}-\frac{2}{r}\Phi(r)=\left[E_{ex}-E_0\right]\Phi(r). \tag{2.9}$$

The binding energy of the exciton, $E_b=E_0-E_{ex}$, is then obtained by solving numerically Eq. (2.9). Notice that this wave equation is similar to one of a hydrogenic atom in an effective isotropic space with the radial part of the Jacobian given by $J_0(r)$ [30]. The properties of this space are generally related to dependence of the Jacobian on r, which according to relation (2.8) is defined to a large extent by the geometry of the heterostructure. If, for example, for any heterostructure this dependence were the power-law, $J_0(r)=Cr^{D-1}$, then the scaling parameter D could be considered as the dimension of the effective space and Eq. (2.9) would coincide with the eigenvalue problem for a hydrogen-like atom in *D*-dimensional space, with D being integer or fractional [28].

It is worth nothing that $J_0(r)$ and $\Phi(r)$ are directly related to the spatial pair correlation function (SPCF), which is defined as the probability density of finding the electron and hole separated by the distance r

$$\mathrm{P}(r) = \left\langle \delta\left(\left|\mathbf{r}_e - \mathbf{r}_h\right| - r\right)\right\rangle . \tag{2.10}$$

In fact, for an uncoupled electron-hole pair the SPCF, $\mathrm{P}(r)$, coincides with the radial part of the Jacobian $J_0(r)$ and it is given by

$$\mathrm{P}_0(r) = \int d\mathbf{r}_e \int f_0^2(\mathbf{r}_e, \mathbf{r}_h)\delta\left(\left|\mathbf{r}_e - \mathbf{r}_h\right| - r\right)d\mathbf{r}_h = J_0(r), \tag{2.11}$$

whereas for exciton:

$$\mathrm{P}(r) = \int d\mathbf{r}_e \int f_0^2(\mathbf{r}_e, \mathbf{r}_h)\Phi^2\left(\left|\mathbf{r}_e - \mathbf{r}_h\right|\right)\delta\left(\left|\mathbf{r}_e - \mathbf{r}_h\right| - r\right)d\mathbf{r}_h = J_0(r)\Phi^2(r) = \chi^2(r). \tag{2.12}$$

In this way the functions $J_0(r)$ and $\chi^2(r)$ give the probability density of finding electron and hole separated by distance r in the uncoupled (free exciton) and coupled (exciton) state, respectively, whereas the function $\Phi^2(r)$ gives the inverse ratio of those probabilities, i.e., $\Phi^2(r) = \mathrm{P}(r)/\mathrm{P}_0(r)$.

2.2 EXCITON IN FRACTIONAL DIMENSIONAL SPACE

In order to give an useful insight into our method, we find out the relation between the fractional dimension of the effective space describing the relative electron-hole pair motion and the actual three-dimensional heterostructure by using the orthogonality condition of the solutions $\Phi_n(r)$, corresponding to the different exciton S-states of the self-consistent differential equation (2.9)

$$\int_0^\infty \Phi_n(r)\Phi_m(r)J_0(r)\,dr = \int \Phi_n(r)\Phi_m(r)\,dV = \delta_{n,m}\,. \tag{2.13}$$

It can be seen that the radial part of the Jacobian volume element, $J_0(r)$, is related to the infinitesimal volume element in the effective vector space of the exciton relative coordinates by $dV = J_0(r)dr$, therefore, it can be considered as the measure of a frontier-surface area of a spherical shell of radii r and $r+dr$. On the other hand, according to relation (2.11), $J_0(r)$ could be easily calculated if the D-dimensional space were homogeneous and isotropic. In this case, all electron-hole separations are equally probable to occur, and consequently $J_0(r)$ is given by the area of a sphere of radius r in a *D*-dimensional space, i.e., $J_0(r) = \mathrm{P}_0(r) = 2\pi^{D/2} r^{D-1} / \Gamma(D/2)$. As a result, the dependence of the SPCF and the Jacobian on *r* is a power-law. However, the real space within the heterostructure is neither isotropic nor homogeneous and therefore the dependence of the Jacobian on *r* is not generally a power-law. Nevertheless, it can be approximated by means of piecewise power-law functions $J_{0s}(r) \approx C_s r^{D_s - 1}$ within different intervals of the electron-hole separations ($r_s < r < r_{s+1}$), considering the scaling parameter D_s as a *running dimension*.

We can also define a *running dimension* for the effective space by using the Mandelbrot's concept of fractals [47]. As the behavior of $J_0(r)$ is not parabolic (three-dimensional case), one can associate to the actual three-dimensional semiconductor system a self-similar fractal object whose fractional dimension D fulfills the relation $J_0(r) = Cr^{D-1}$ [30]. Since due to the confinement of the heterostructure the function $J_0(r)$ has no a power-law dependence on r at all, we assume that the parameters C and D in the above scaling

equation also depend on r, and consequently $J_0(r)$ will be related to the *running dimension* $D^*(r)$ as follow

$$J_0(r) = C(r) r^{D^*(r)-1}. \tag{2.14}$$

Here we consider that the functions $C(r)$ and $D^*(r)$ vary more slowly than any power function. In this way the *running dimension* is defined as follow

$$D^*(r) = 1 + r\frac{d \ln J_0(r)}{dr}. \tag{2.15}$$

In order to illustrate the concept of non-fixed fractional dimension, we calculate the functions $J_0(r)$ and $D^*(r)$ for an exciton in QW, cylindrical QWW and in spherical QD for the square-well potential in the absence of external field. In this case Eq. (2.3) is separable and one can calculate $J_0(r)$ directly by using the relation (2.11) and the well-known analytical expressions for the ground state wave functions of the electron and the hole in the respective heterostructure [30].

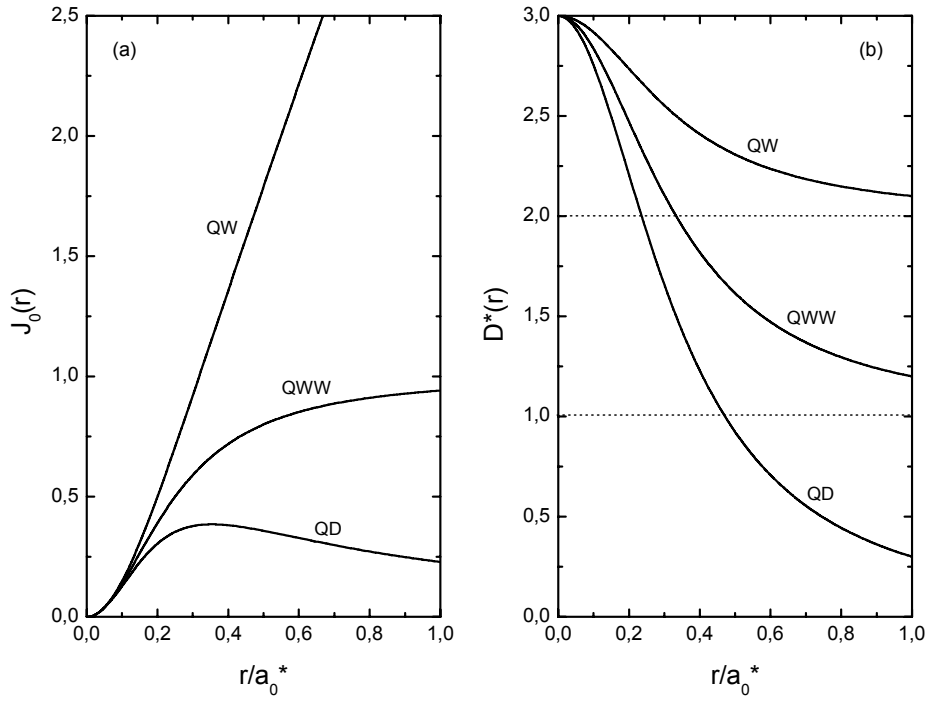

Figure 2.1 The radial part of the Jacobian (a) and running dimension (b) dependences on the electron-hole separation in QW, cylindrical QWW and spherical QD.

Figure 2.1 (a) shows the typical behavior of the radial part of the Jacobian for the three heterostructures. For small values of the electron-hole separations, as the electron-hole distance is essentially smaller than the size of the heterostructure, the tree curves behave as parabolic ($J_0 \sim r^2$) similar to the three-dimensional case. As the electron-hole distance increases and becomes greater than the heterostructure size, the curves transform into a linear function ($J_0 \sim r$) for a QW, a constant ($J_0 \sim r^0$) for QWW and into a decreasing exponential function ($J_0 \sim 0$) for QD, corresponding to the two-one and zero-dimensional cases. The corresponding dependencies of the *running dimension* on the relative coordinate of the exciton are shown in Fig. 2.1 (b). As expected, the dimension falls from 3 for small electron-hole distances to 2 in QW, to 1 in QWW and to 0 in QD, as the electron-hole separation becomes larger than the size of the corresponding heterostructure. Such a

dependence is typical of quasi-two, -one and –zero-dimensional heterostructures, respectively.

Additionally, we can define the *fractional dimension* as the average of the *running dimension* given by Eq. (2.15). Assuming that the probability density of finding the electron and hole separated by the distance r is given by the radial part of a hydrogen-like atom wave function of the *ns*-state in D-dimensional space, $R_n\left(r,D\right)$, we define the *fractional dimension* as:

$$\bar{D}=\int_0^\infty D^*\left(r\right)R_n^2\left(r,D^*\left(r\right)\right)J_0\left(r\right)dr\Bigg/\int_0^\infty R_n^2\left(r,D^*\left(r\right)\right)J_0\left(r\right)dr, \tag{2.16}$$

where

$$R_n\left(r,D\right)=\exp\left(-\kappa r\right)M\left(1-n,\ D-1,\ 2\kappa r\right);\ \kappa=\frac{1}{n+\left(D-3\right)/2}, \tag{2.17}$$

with $M\left(a,b,z\right)$ being the confluent hypergeometric function [26]. Once $\bar{D}$ is calculated, the exciton binding energy E_b and the corresponding wave function $\Psi_n\left(\mathbf{r}_e,\mathbf{r}_h\right)$ can be obtained in a straightforward way through [30]:

$$E_b=\frac{4}{\left(n+\left(\bar{D}-3\right)/2\right)^2};\ \Psi_n\left(\mathbf{r}_e,\mathbf{r}_h\right)=f_0\left(\mathbf{r}_e,\mathbf{r}_h\right)R_n\left(r,\ \bar{D}\right). \tag{2.18}$$

Thus, there are two different approaches to solve the problem of the exciton S-states in heterostructures. First solving the one-dimensional wave equation (2.9) by using any known numerical procedure, in particular, the trigonometric sweep method [48]), and second by using Eq. (2.18) previous calculation of the *fractional dimension* (2.16). The latter is more simple but breaks down when the confinement is too strong [28].

2.3 THE COFINEMENT POTENTIAL

Potentials that confine electrons and holes in QWs, QWWs and QDs, can possess various shapes depending on their origin and the structure of the semiconductor system [16]. The knowledge of the realistic profile of the confinement potential is important in theoretical studies. The potential can be either obtained from the first-principles calculations or simply assumed in some parametrized form, which allow us to model its shape. When using the first method, it also appears to be helpful to find some parametrized analytic form of the confinement potential, which is useful in further applications, e.g. in the Hartree-Fock method [49]. The confinement potential is usually modeled by the two simple forms: either the square-well (rectangular) or the parabolic (harmonic oscillator) potential with finite and infinite depth, respectively. Nevertheless, as it results from the numerical solution of the Poisson equation, a realistic potential within quantum-well heterostructures is nearly parabolic at the center of the well and becomes non-parabolic at the structure boundary. Furthermore, the confining potential should possess a finite depth and range, which results from the finite band offset and the finite size of the heterostructure, and a variable softness, which allow us to take into account a compositional modulation (alloying) and strain effects in the semiconductor structure. For the purpose of this study, we propose the following confinement potential which fulfills the above-mentioned conditions:

$$V(q) = V_0\Theta(-q,-q_0,W) + V_0\Theta(q,q_0,W). \tag{2.19}$$

Here q is a generalized coordinate and $\Theta(q,q_0,W)$ is a soft-step function that has continuous first and second derivatives in all space and it is defined as follows:

$$\Theta(q,q_0,W)=\begin{cases}0 & q<q_0-W\\ \left[(q-q_0)^2/W^2-1\right]^2 & q_0-W\le q<q_0\\ 1 & q\ge q_0\end{cases}. \tag{2.20}$$

It can be seen that $\Theta(q,q_0,W)$ increases smoothly from 0 at the point $q=q_0-W$ up to 1 at the point $q=q_0$, and it turns into the Heaviside function as $W\to 0$. The parameter W can be associated with a variable softness at the structure boundary, and by varying its value different shapes of the confinement potentials can be obtained. For instance, for a QW the potential is defined as

$$V(z)=V_0\Theta(-z,-L/2,W)+V_0\Theta(z,L/2,W). \tag{2.21}$$

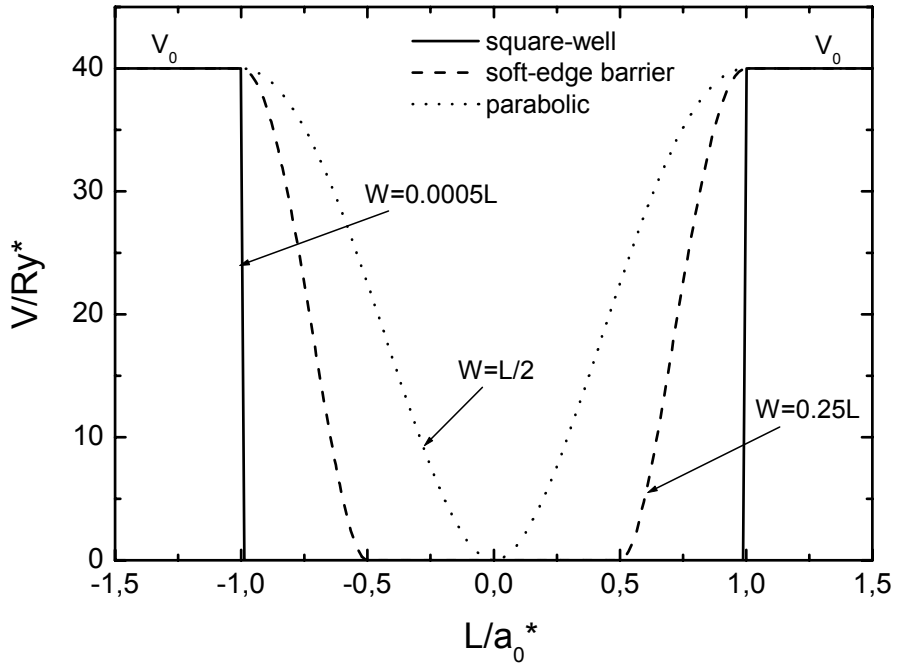

Figure 2.2 Confinement potentials for a QW of width 200 Å modeled by using equation (2.21).

Different potential profiles are shown in Fig. 1 for a QW of width 200 Å. Here W determines the thickness of a layer at the structure boundary in which the potential falls off

from $V = V_0$ outside to $V = 0$ inside the well. This function describes for $W = 0$ the almost rectangular potential and for $W = L/2$ the almost parabolic potential with a finite barrier. It is also possible to obtain different soft-edge barrier potentials as $0 < W < L/2$.

In order to model a cylindrical nanotube of internal and external radii R_i (core radius) and R_e (wire radius), and corresponding height barriers V_i and V_e, the potential is defined as

$$V(r) = V_i \Theta(-r, -R_i, W) + V_e \Theta(r, R_e, W), \tag{2.22}$$

with r being the in-plane radial coordinate. The models of square-well, parabolic and core-repulsive potential (nanotube-like wire) are displayed in Fig. 2.3.

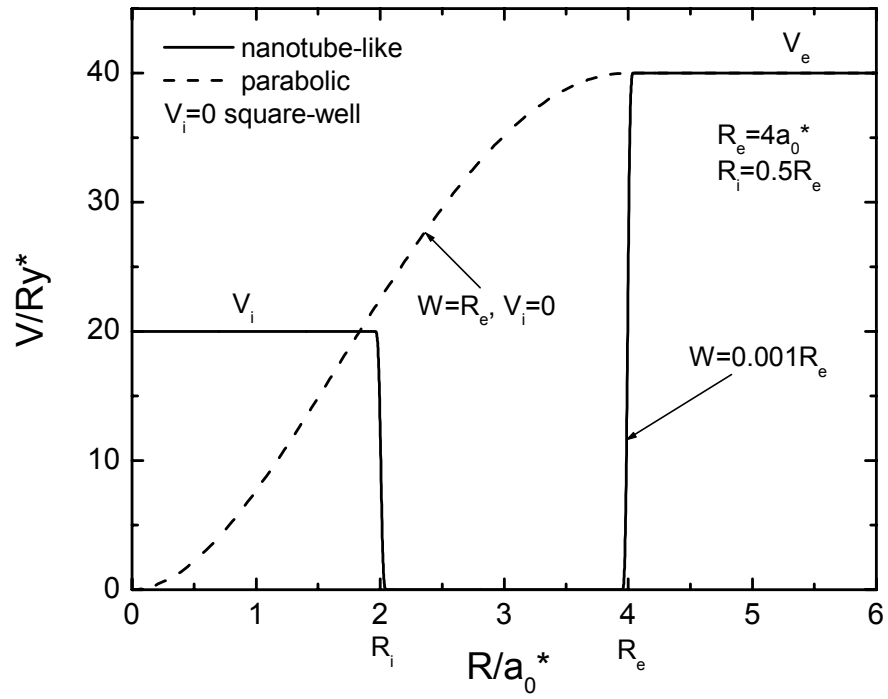

Figure 2.3 Different models of the confinement potential in a quantum wire of radius 400 Å.

The parameter W determines the thickness of the layers in which the potential falls off from V_i inside the core to 0 inside the wire, and from V_e outside the wire to 0 inside the wire. In

particular, if $V_i = 0$ the confining potentials for a cylindrical QWW are obtained, from the rectangular to the parabolic when W goes from 0 to R_e.

In the case of an spherical quantum dot the potential can be modeled by

$$V(r) = V_0 \Theta(r, R, W), \tag{2.23}$$

with r being the radial coordinate, R the dot radius and W the parameter that determines the thickness of a transition region in which the potential falls off from $V = V_0$ outside the dot to $V = 0$ inside the dot.

3. APPLICTATIONS FOR A MODEL WITHOUT MAGNETIC FIELD

Turning into applications of the method, first we consider an exciton in different heterostructures of GaAs-(Ga, Al)As without the presence of magnetic field. In our calculations we use the material parameters pertaining to GaAs $\varepsilon = 12.53$, $m_e^* = 0.067 m_0$ with m_0 being the bare electron mass. For the light-hole masses are $m_z^* = 0.08 m_0$ and $m_\perp^* = 0.21 m_0$, while for the heavy-hole are $m_z^* = 0.45 m_0$ and $m_\perp^* = 0.10 m_0$. The isotropic hole mass is calculated as $m_h^{*-1} = (2/3) m_\perp^{*-1} + (1/3) m_z^{*-1}$ [8, 17], in this case the reduced mass is $\mu = 0.0447 m_0$ and $\mu = 0.0449 m_0$ for the heavy- and light-hole exciton respectively. Since both reduced masses are very close to each other only results for one kind of exciton are presented. To determine the energy band-gap discontinuity in QW and in QWW we use the empirical formulae $\Delta E_g = (1.155x + 0.37x^2) eV$ and $\Delta E_g = (1.360x + 0.22x^2) eV$ respectively, with 60% of ΔE_g contribution to the conduction-band and 40% of ΔE_g contribution to the valence band discontinuity [8]. For QD we use the formula $\Delta E_g = (1.087x + 0.438x^2) eV$ with 65% of ΔE_g contribution to the conduction-band and 35% of ΔE_g contribution to the valence-band discontinuity [13].

3.1 EXCITON IN SYMMETRICAL STEP QUANTUM WELLS

We consider an exciton in a GaAs-(Ga, Al)As QW without the presence of magnetic field. In this type of heterostructures the particles undergoes confinement only along of the growth direction, and the confining potential can be described by using Eq. (2.21). Excluding from consideration the free motion of the exciton center-of-mass in the *x*-*y* plane, the Hamiltonian (2.1) of the system can be written in cylindrical coordinates as

$$H_0 = H_e + H_h + H_\rho - 2\tau / r_{eh} \quad (\tau = 0,1); \tag{3.1}$$

$$H_e = -\eta_e \frac{\partial^2}{\partial z_e^2} + V_e(z_e); \quad H_h = -\eta_h \frac{\partial^2}{\partial z_h^2} + V_h(z_h); \quad H_\rho = \eta_h \left(-\frac{1}{\rho} \frac{\partial}{\partial \rho} \rho \frac{\partial}{\partial \rho} \right), \tag{3.2}$$

where $\rho = \sqrt{(x_e - x_h)^2 + (y_e - y_h)^2}$, $r_{eh} = \sqrt{\rho^2 + (z_e - z_h)^2}$ are the in-plane and spatial distances between electron and hole respectively, while $V_e(z_e)$ and $V_h(z_h)$ are the confinement potentials of the heterostructure given by the relation (2.21).

The solution of the eigenvalue problem (2.3) for the Hamiltonian (3) is easily obtained as:

$$f_0(\mathbf{r}_e, \mathbf{r}_h) = f_e(z_e) f_h(z_h); \quad E_0 = E_e + E_h, \tag{3.3}$$

where $f_e(z_e)$ and $f_h(z_h)$ are solutions of the one-dimensional equations

$$-\eta_e \frac{\partial^2 f_e(z_e)}{\partial z_e^2} + V_e(z_e) f_e(z_e) = E_e f_e(z_e); \tag{3.4}$$

$$-\eta_h \frac{\partial^2 f_h(z_h)}{\partial z_h^2} + V_h(z_h) f_h(z_h) = E_h f_h(z_h), \tag{3.5}$$

with E_e and E_h being the lowest energies of the electron and hole in the QW respectively. Once the one-dimensional wave equations (3.4) and (3.5) are solved, the function $J_0(r)$

can be calculated through the two-dimensional integrals which arise from the general expression (2.11) after integrating over the Euler angles:

$$J_0(r) = 2\pi r \int_{-\infty}^{\infty} f_e^2(z_e)\, dz_e \int_{-r}^{r} f_h^2(z_e + z)\, dz\,. \tag{3.6}$$

The ground state binding energy is obtained from Eq. (2.9) by using the trigonometric sweep method [48], and the *running dimension* calculated by using the relation (2.15).

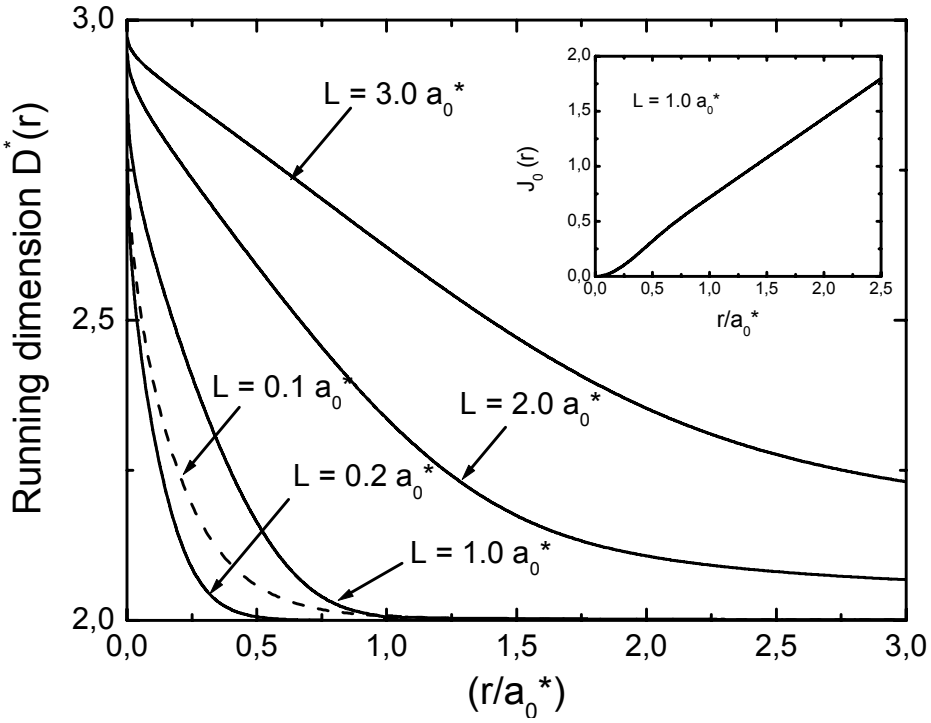

Figure 3.1 Running dimension as a function of the electron-hole separation for an exciton in a $GaAs/Ga_{0.7}Al_{0.3}As$ QW and for different well width.

Figure 3.1 shows the running dimension D^* as a function of the electron-hole separation r for the exciton ground state in a square-well $GaAs/Ga_{0.7}Al_{0.3}As$ QW and for different well width. The inset in the same plot displays the typical behavior of the radial part of the Jacobian $J_0(r)$ for a quantum well of width $1.0\,a_0^*$. As explained in section 2.2, when the electron-hole distance is smaller than the well width $J_0 \sim r^2$ (three-dimensional case) and

when it is larger $J_0 \sim r$ (two-dimensional case). It can also be seen from Fig. 3.1 that the *running dimension* $D^*(r)$ falls from 3 for small electron-hole separations to 2 as this distance is comparable to the well width. Such a dependence is characteristic of a two-dimensional space as we would expect for a quasi-two dimensional quantum well. Notice that, as the well size is greater than a critical width $\left(0.2\,a_0^*\right)$ the slope of the curves becomes less pronounced because of the leakage of the wave function into the barriers (dotted line). Furthermore, in the limits $L \to \infty$ and $L \to 0$ the corresponding slope becomes almost horizontal and the dimension tends to three for any value of the electron-hole separation.

In order to check the accuracy of the method, we calculate the exciton ground state binding energy as a function of the well width, for the square-well and soft-edge barrier potentials, the corresponding results are showed in Fig. 3.2. Our results (lower curve) for the rectangular potential are compared with those from Ref. [28] (solid circles). There is an insignificant discrepancy between both sets of results which can be ascribed to the fact that we assume for simplicity an isotropic model of the hole mass, whereas in Ref. [28] calculation for light- and heavy-hole exciton was performed. The inset in the same figure shows the profile of the potential for three different thickness of the transition region at the heterostructure boundary corresponding to the almost rectangular $(W/L = 0.01)$, soft-$(W/L = 0.1)$ and very soft-edge $(W/L = 0.3)$ barrier potentials.

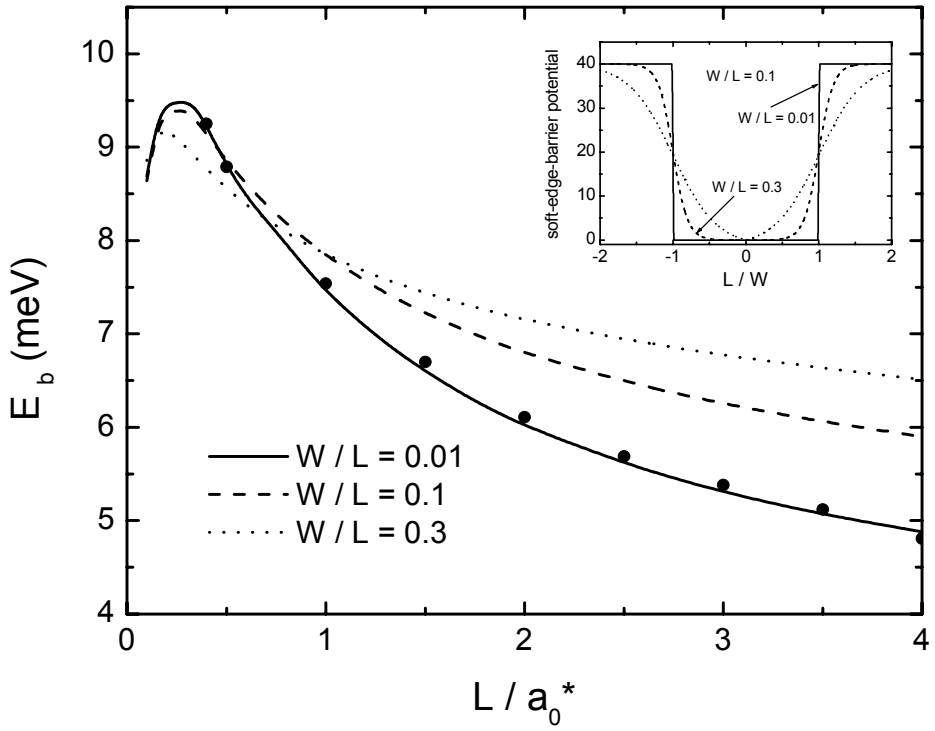

Figure 3.2 Ground state binding energy of an exciton in a GaAs/$Ga_{0.7}Al_{0.3}As$ QW as a function of the well width for different soft-edge barrier potentials. Solid circles correspond to theoretical calculations from Ref. [28].

The binding energy curves crossover in the region $0.5 < L/a_0^* < 1.5$ is evident. It is apparent that for intermediate and large well widths $L/a_0^* > 1.5$ the confinement is not too strong, and for the rectangular potential the exciton energy level is deeper than the level for the smooth- and the very smooth-edge barrier potentials respectively. As a result, in that interval the potential corresponding to $W/L = 0.3$ gives the largest binding energy followed by the soft-edge barrier $(W/L = 0.1)$, whereas the almost rectangular $(W/L = 0.01)$ gives the smallest exciton binding energy. The opposite occurs in the region $L/a_0^* < 0.5$ where the rectangular potential gives the largest binding energy. In this case, as the well width decreases the exciton level is pushed out faster than the level for the soft and very soft

edge-barrier potentials respectively. Consequently for the rectangular potential, the wave function starts leaking steadily into the barriers first than the exciton wave functions corresponding to the other two potentials.

We also calculated the ground state binding energy of an exciton in a $Ga_{0.55}Al_{0.45}As/Ga_{0.8}Al_{0.2}As/GaAs/Ga_{0.8}Al_{0.2}As/Ga_{0.55}Al_{0.45}As$ double-step quantum well consisting of a small rectangular well of length L_1 inside of a large one of length L [48]. The corresponding results are displayed in Fig. 3.3. From the plot one can see the existence of a peak and a shoulder in the curves of the binding energy for the double-step QW with $L_1 = 0.15L$ and $L_1 = 0.20L$. In these cases, as the well width decreases, the wave function

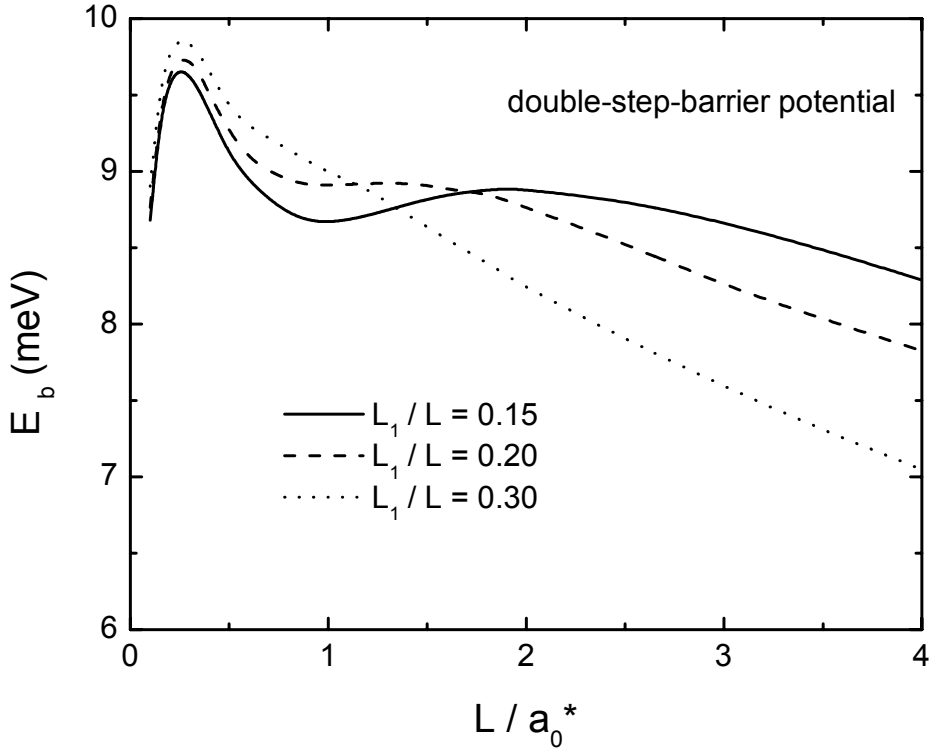

Figure 3.3 Exciton ground state binding energies as a function of the well width in a $GaAs/Ga_{0.8}Al_{0.2}As/Ga_{0.55}Al_{0.45}As$ double-step QW and for several values of the internal well width L_1.

first leaks into the interior barrier region giving rise to a this kind of shoulder which is not too pronounced because the exciton is still confined. With further decreasing of the well width, the exciton level is pushed up and the exciton binding energy increases up to a maximum value (peak) corresponding to a critical width for which the wave function starts leaking into the exterior barriers region until the 3D character of the wave function is restored. When the inner well is sufficiently wide, the exciton does not feel the presence of it and for that reason the shoulder in the binding energy curve vanishes (dotted line), that is, the system behaves as a single quantum well.

3.2 EXCITON IN CYLINDRICAL QUANTUM-WELL WIRES

We consider an exciton in a cylindrical GaAs-(Ga, Al)As QWW without the presence of magnetic field. We assume that the wire is sufficiently long so that the exciton motion along the wire axis is translationally symmetric and therefore the confinement potential depends only on the in-plane radial coordinate. The Hamiltonian (2.1) of this system can be written in cylindrical coordinates as

$$H_0 = H_e + H_h - 2\tau / r_{eh}, \quad (\tau = 0,1) \tag{4.1}$$

$$H_e = -\eta_e \frac{1}{\rho_e}\frac{\partial}{\partial \rho_e}\rho_e \frac{\partial}{\partial \rho_e} + V_e(\rho_e); \quad H_h = -\eta_h \frac{1}{\rho_h}\frac{\partial}{\partial \rho_h}\rho_h \frac{\partial}{\partial \rho_h} + V_h(\rho_h), \tag{4.2}$$

with $V_e(\rho_e)$ and $V_h(\rho_h)$ being the confinement potentials for the electron and hole in the QWW given by the relation (2.22).

The solution of the eigenvalue problem (2.3) corresponding to the Hamiltonian (4) can easily be obtain as:

$$f_0(\mathbf{r}_e,\mathbf{r}_h)=f_e(\rho_e)f_h(\rho_h);\quad E_0=E_e+E_h, \tag{4.3}$$

where $f_e(\rho_e)$ and $f_h(\rho_h)$ are solutions of the one-dimensional wave equations:

$$-\eta_e\frac{1}{\rho_e}\frac{\partial}{\partial\rho_e}\rho_e\frac{\partial f_e(\rho_e)}{\partial\rho_e}+V_e(\rho_e)f_e(\rho_e)=E_e f_e(\rho_e); \tag{4.4}$$

$$-\eta_h\frac{1}{\rho_h}\frac{\partial}{\partial\rho_h}\rho_h\frac{\partial f_h(\rho_h)}{\partial\rho_h}+V_h(\rho_h)f_h(\rho_h)=E_h f_h(\rho_h), \tag{4.5}$$

with E_e and E_h being the lowest energies of the electron and hole in the wire respectively. Once the one-dimensional equations (4.4) and (4.5) are solved, the Jacobian $J_0(r)$ can be calculated through the following two-dimensional integral which arise from the relation (2.11) after integrating over the Euler angles and z-coordinates:

$$J_0(r)=4\pi r\int_0^{\infty}f_e^2(\rho_e)\rho_e d\rho_e\int_{\max\{0,\rho_e-r\}}^{\rho_e+r}K\left(\frac{a}{b}\right)\frac{f_h^2(\rho_h)\rho_h}{b}d\rho_h, \tag{4.6}$$

$K(x)$ is the complete elliptic integral of first kind, while $a=\min\left\{4\rho_e\rho_h,\sqrt{r^2-(\rho_e-\rho_h)^2}\right\}$ and $b=\max\left\{4\rho_e\rho_h,\sqrt{r^2-(\rho_e-\rho_h)^2}\right\}$. The ground state binding energy is obtained from Eq. (2.9) by using the same numerical method [48] as for the quantum well.

The ground state binding energy of an exciton in a GaAl/$Ga_{0.7}Al_{0.3}As$ QWW for a model with rectangular and soft-edge barrier potentials is calculated, and the corresponding results are presented in Fig. 3.4. The plot displays the binding energy as a function of the wire

radius. Our results for the rectangular potential (solid lines) are in excellent agreement with those by Li et al. [8] (solid circles).

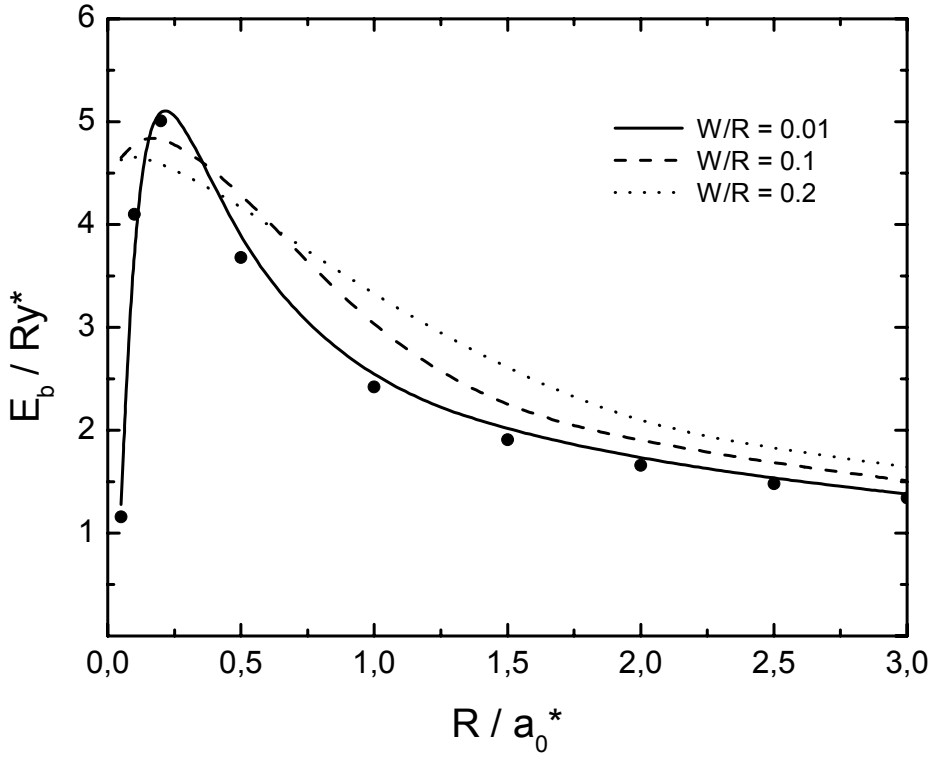

Figure 3.4 Ground state binding energy of an exciton in a GaAs/$Ga_{0.7}Al_{0.3}As$ QWW as a function of the wire radius, for a model with rectangular potential (solid lines) and soft-edge barrier (dashed and dotted lines). Solid circles (•) correspond to calculations from Ref. [8].

The binding energy curves crossover in the region $0.3 < R/a_0^* < 0.7$ is evident. For the rectangular potential and for intermediate and large wire radius ($R/a_0^* > 0.7$) the exciton level is deeper than the level for the soft- and very soft-edge barrier potentials respectively. Consequently, in that interval the potential corresponding to $W/R = 0.2$ gives the largest binding energy followed by the soft-edge barrier $W/R = 0.1$, whereas the almost rectangular $W/R = 0.01$ gives the lowest exciton binding energy. The opposite happens in the region $R/a_0^* > 0.3$ where the rectangular potential gives the largest binding energy. In this case, as

the wire radius decreases the exciton level is pushed out faster than the level for the soft- and very soft-edge barrier potentials respectively. As a result, for the rectangular potential the exciton wave function overflow first than the wave functions corresponding to the other two potentials.

To our knowledge, no theoretical results on the excitonic spectra in QWWs with a double-step potential have been reported until now. We apply our method to analyze the ground state of an exciton located at the axis of a GaAs/$Ga_{0.8}Al_{0.2}As$/$Ga_{0.55}Al_{0.45}As$ coaxial QWW. The confinement potential is a double-step quantum well consisting of a small well of length R_1 inside of a large one of length R. In this structure the potential changes from 0 in GaAs to V_1 in $Ga_{0.8}Al_{0.2}As$ and to V_2 in $Ga_{0.55}Al_{0.45}As$. The results obtained are displayed in Fig. 3.5, where the exciton binding is plotted as a function of the wire radius R, for several values of the inner radius R_1. From the plot one can see the existence of two maxima (peaks) in the curves of the binding energy for the structures with $R_1 = 0.2R$ and $R_1 = 0.3R$. In both cases, as the wire radius diminishes the wave function first overflow the inner well giving rise to the minor peak. With further radius decreasing, the exciton level is pushed up and the binding energy starts increasing again until it reaches a maximum (main peak) afterwards the wave function overflow the external well.

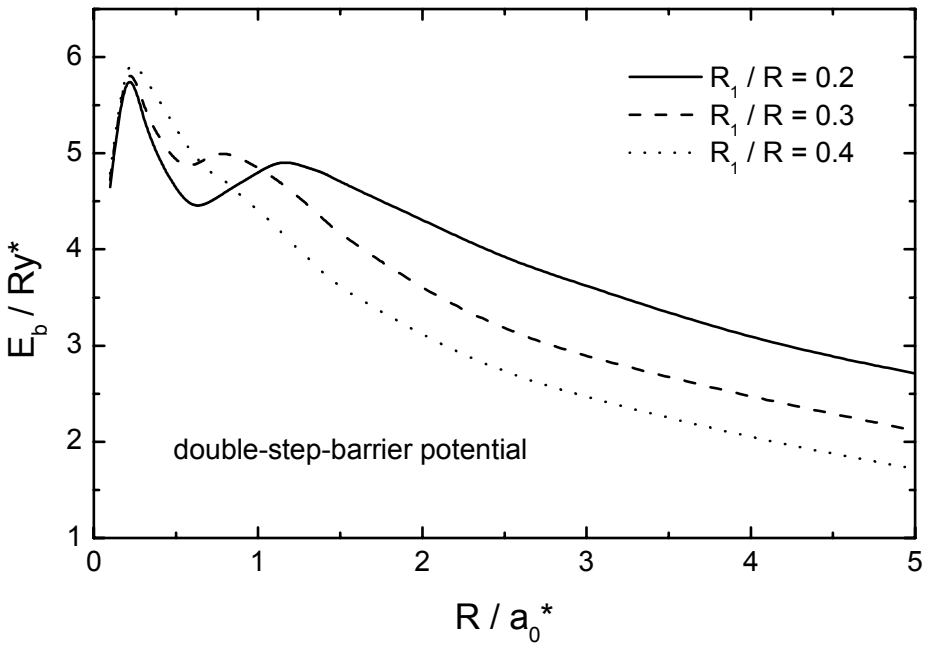

Figure 3.5 Ground state binding energy of an exciton in a GaAs/$Ga_{0.8}Al_{0.2}As$/$Ga_{0.55}Al_{0.45}As$ coaxial QWW as a function of the wire radius, for a model with double-step quantum well potential.

3.3 EXCITON IN SPHERICAL QUANTUM DOTS

We consider an exciton in a spherical GaAs-(Ga, Al)As QD without the presence of magnetic field, so that the confinement potential depends only on the radial coordinate. The Hamiltonian (2.1) of this system can be written in spherical coordinates as

$$H_0 = H_e + H_h - 2\tau/r_{eh} \quad (\tau = 0,1); \tag{5.1}$$

$$H_i = -\eta_i \nabla_i^2 + V_i(r_i) \quad (i = e,h), \tag{5.2}$$

where r_i are the particle distances from the QD center, and $V_i(r_i)$ are the corresponding confining potentials which are given by Eq. (2.23).

The solution of the eigenvalue problem (2.3) for the Hamiltonian (5) is easily obtained as

$$f_0(\mathbf{r}_e, \mathbf{r}_h) = f_e(r_e) f_h(r_h); \quad E_0 = E_e + E_h, \tag{5.3}$$

where $f_e(r_e)$ and $f_h(r_h)$ are solutions of the one-dimensional wave equations:

$$-\eta_e \frac{1}{r_e} \frac{\partial}{\partial \rho_e} r_e \frac{\partial f_e(r_e)}{\partial r_e} + V_e(r_e) f_e(r_e) = E_e f_e(r_e); \tag{5.4}$$

$$-\eta_h \frac{1}{r_h} \frac{\partial}{\partial \rho_h} r_h \frac{\partial f_h(r_h)}{\partial r_h} + V_h(r_h) f_h(r_h) = E_h f_h(r_h), \tag{5.5}$$

with E_e and E_h being the lowest energies of the electron and hole in the dot respectively. Once the one-dimensional equations (5.4) and (5.5) are solved, the Jacobian $J_0(r)$ can be calculated through the following two-dimensional integral which arise from the relation (2.11) after integrating over the Euler angles:

$$J_0(r) = 8\pi^2 r \int_0^{\infty} r_e f_e^2(r_e) dr_e \int_{|r_e - r_{eh}|}^{r_e + r_{eh}} r_h f_h^2(r_h) dr_h. \tag{5.6}$$

The ground state exciton binding energy is also obtained from Eq. (2.9) by using the same numerical procedure [48].

The ground state binding energy of an exciton in a spherical GaAl/$Ga_{0.7}Al_{0.3}As$ QD for a model with rectangular and soft-edge barrier potentials is calculated, and the corresponding results are presented in Fig. 3.6. The plot displays the binding energy as a function of the dot radius. As the radius decreases, the exciton wave function is compressed into the QD and the binding energy increases because of the enhancement of the Coulomb attraction, until it reaches a maximum corresponding to a confinement threshold. With further decreasing of the dot radius, the exciton wave function leaks into the barrier region and

consequently the binding energy diminishes sharply from its maximum value up to the exciton energy in bulk (1 *Ry**) as the exciton assumes more of its 3D-like nature.

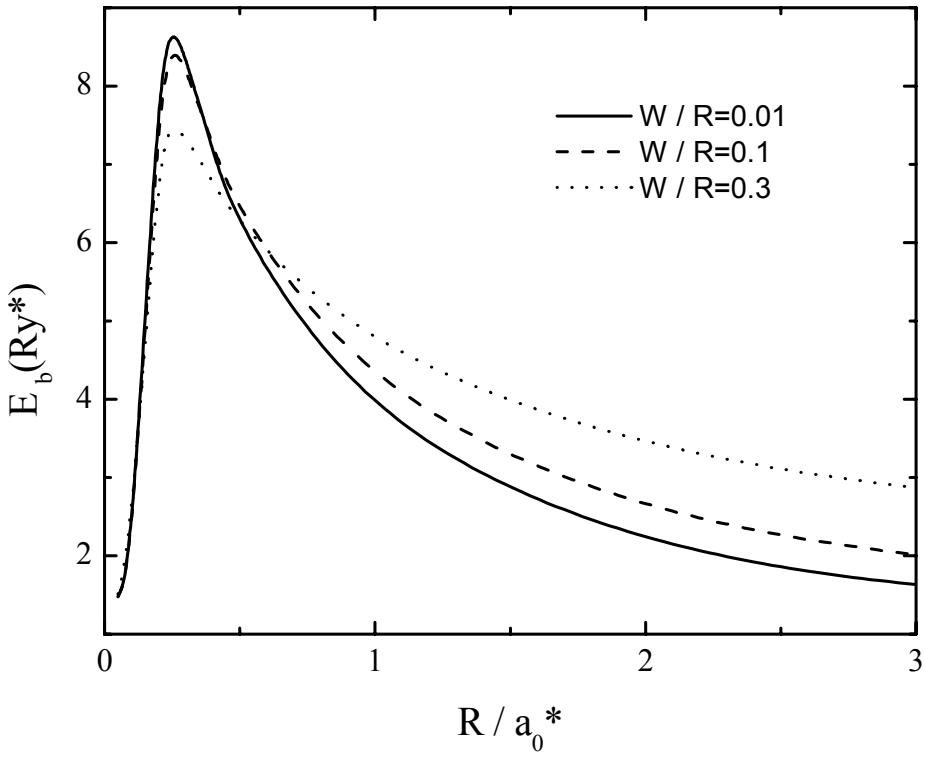

Figure 3.6 Ground state binding energy of an exciton in a GaAs/$Ga_{0.7}Al_{0.3}As$ spherical QD as a function of the dot radius for different soft-edge barrier potentials.

The curves crossover in the region $0.4 < R/a_0^* < 0.7$ is evident. It is apparent that for intermediate and large values of the QD radius $\left(R/a_0^* > 0.7\right)$ the excitonic orbital confinement, due to the rectangular potential $\left(W/a_0^* = 0.01\right)$, is smaller than for the smooth- $\left(W/a_0^* = 0.1\right)$ and very smooth-edge $\left(W/a_0^* = 0.3\right)$ barrier potentials. Because of this, in that region the latter gives the largest binding energy and the rectangular the smallest one. The contrary occurs in the region $\left(R/a_0^* < 0.4\right)$, as the dot radius decreases, the exciton energy level is pushed up towards the upper part of the conduction band where

the rectangular potential gives the strongest confinement. Therefore, in that interval the very smooth-edge barrier potential gives the smallest binding energy.

We also performed calculations for an exciton in a GaAs/$Ga_{0.8}Al_{0.2}As$/$Ga_{0.55}Al_{0.45}As$ spherical QD. The confinement potential is the same described for the coaxial wire but in radial direction with R being the radius of the dot. The results obtained are displayed in Fig. 3.7, where the exciton binding is plotted as a function of the dot radius R, for several values of the inner radius R_1.

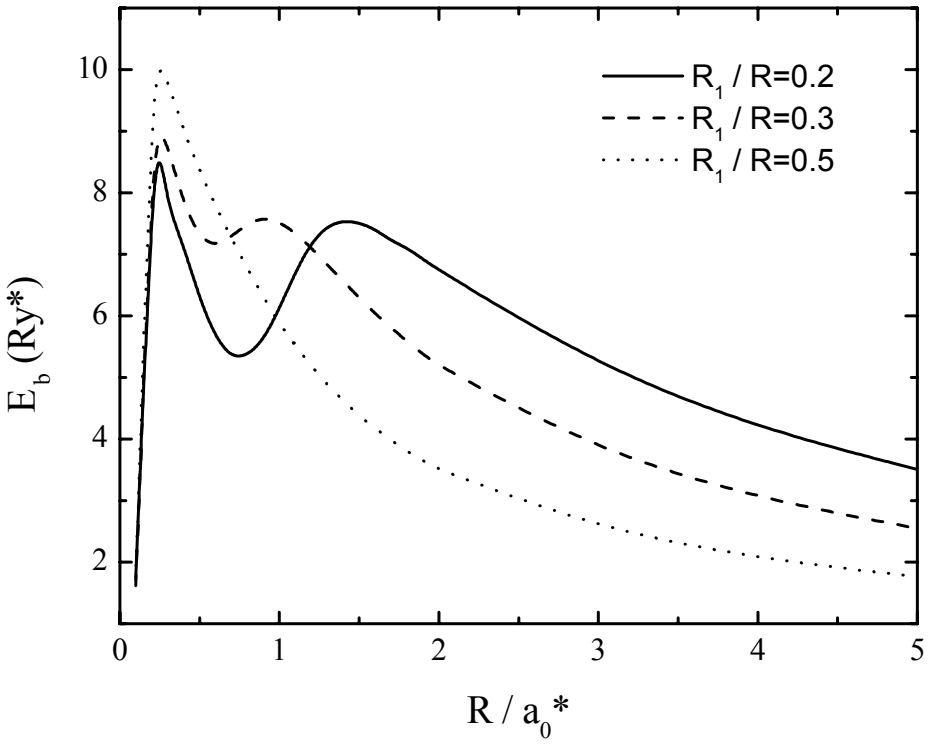

Figure 3.7 Ground state binding energy of an exciton in a GaAs/$Ga_{0.8}Al_{0.2}As$/$Ga_{0.55}Al_{0.45}As$ spherical QD as a function of the wire radius, for a model with double-step quantum well potential.

As happened for exciton in QW and QWW, the curves of the binding energy has two maxima (peaks), the minor one is associated with the overflow of the wave function from the inner well while the main peak is related to the overflow of the function from the

external well. When the internal well becomes wider the system behaves as single quantum well and therefore only one maximum is observed.

4. POLARONIC EXCITON IN QUANTUM-WELL WIRES AND NANOTUBES

In this part of the thesis we investigate the effect of the longitudinal-optical phonon field on the binding energies of excitons in quantum wells, well-wires and nanotubes based on ionic semiconductors by using the method developed previously

4.1 INTRODUCTION

In the past decade, there has been increasing interest in the study of wide-gap II-VI semiconductor heterostructures, in particular quantum wells (QWs) structures have been studied both theoretically and experimentally [50-53]. These systems offer a variety of opto-electronic device applications in the visible and ultraviolet wavelength regions, and in high-temperature electronics. It is well known that the electron longitudinal-optical (LO) phonon interaction is an important factor influencing the physical properties of polar crystals. The effect of such influence becomes stronger as the dimensionality of the system reduces [54]. The exciton-phonon interaction in bulk ionic semiconductors has been a subject of a numerous investigations in contrast to its counterpart in systems with reduced dimensionality. Different groups [55-57] have calculated the binding energies of excitons in quantum well heterostructures in the presence of LO-phonon field. Most of them assume the Fröhlich Hamiltonian [58], which is valid for bulk semiconductors or wide wells, to describe the electron (hole) phonon interaction. All calculations show that exciton binding energies are enhanced, with respect to the case when a screened Coulomb potential is

considered. However, it has been demonstrated that some approaches overestimate the exciton binding energy, especially in weakly ionic heterostructures, e.g. GaAs/GaAlAs [57]. One of the most useful techniques to deal with this problem is to derive an expression for the effective interaction potential between the electron and the hole taking into account their interactions with the LO-phonon field of the crystal lattice. Following such approach different interaction potentials have been obtained. Particularly, the Pollmann-Bütner [59] and Aldrich-Bajaj [57, 60, 61] potentials have proven to describe very well the electron-phonon interaction. The values of the exciton binding energies calculated using these potentials are in good agreement with the available experimental results.

On the other hand, Thilagam [62] derived the analytical expression of the Fröhlich-like Hamiltonian for the interaction between an exciton and an optical phonon in the fractional-dimensional space in order to study the exciton line widths in the GaAs/GaAlAs QWs. The fractional-dimensional space technique was first applied by He [25], who using the hydrogen-like Hamiltonian in effective fractional space proposed by Stillinger [26] treated the interband optical transitions and bound excitons in strongly anisotropic media. This model has been successfully used to describe excitons in semiconductor heterostructures [27-28] in the weak and intermediate confinement regime. Though such approach allows a reduction of the computational time to obtain the exciton energies with a reasonable accuracy, it has been established that this breaks down when the confinement is too strong, e.g. quantum wells in the presence of strong magnetic fields, quantum well wires and quantum dots of a very small sizes [28]. Recently, a new method based on the fractional-dimensional model was proposed to study the ground state of neutral (D^0) charged (D^-) donors and excitons in heterostructures semiconductors [29-30]. The method provides a

simple and unified procedure for calculating the impurities and excitons ground state binding energies in different heterostructures with arbitrary confining potential. Its accuracy has been tested by comparison with theoretical calculations from Monte Carlo and Variational methods and was proven to work very well even when the carriers confinement is stronger.

We extend the method developed previously for neutral and charge donor [29, 30] to study the ground state of excitons, in quantum-wells heterostructures, where the Coulomb potential is replaced by the Aldrich-Bajaj (AB) effective potential for the exciton LO-phonon interaction [57, 60]. First we present the model and discuss how the approach is used to solve the problem of excitons in quantum wells (QWs) and quantum well wires (QWWs). Second, we present the results for different heterostructures and compare them with available theoretical and experimental data. We also consider different shape of the confinement potentials for the same type of hetereosturcture (QW and QWW). Finally, we present our remarks and conclusions.

4.2 THEORETICAL MODEL

The dimensionless Hamiltonian for a correlated electron-hole pair confined in semiconductor heterostructure in the presence of the LO-phonon field of the crystal lattice can be written as:

$$H = H_0\left(\mathbf{r}_e, \mathbf{r}_h\right) - V_{ex}; \qquad H_0\left(\mathbf{r}_e, \mathbf{r}_h\right) = H_e\left(\mathbf{r}_e\right) + H_h\left(\mathbf{r}_h\right); \tag{4.1}$$

$$H_i(\mathbf{r}_i) = -\eta_i \nabla_i^2 + V_i(\mathbf{r}_i) + \alpha_i \hbar\omega\,, \tag{4.2}$$

where $H_i(\mathbf{r}_i)$ with $i = e,h$ describes the motion of the particle-polaron confined in the heterostructure and V_{AB} is the effective electron-hole potential which takes into account the interaction with the LO-phonon field. As units of length and energy we use the effective donor Bohr radius $a_{\mathrm{B}} = \varepsilon_0 \hbar^2 / m_e e^2$ and the electron effective donor Rydberg $R_y = e^2 / 2\varepsilon_0 a_B$, respectively, where m_e is the electron effective band mass and ε_0 the static dielectric constant. The parameter η is defined as $\eta_i = m_e / m_i^*$ $(i = e,h)$ with m_i^* being the electron (hole) polaron mass, which is related to the band mass by $m_i^* = m_i (1 + \alpha_i/12)/(1 - \alpha_i/12)$. Here the hole polaron mass is calculated by using a spherical hole mass approximation [8]. For V_{AB} we consider the effective potential derived by Aldrich and Bajaj [57, 60] which takes into account the polaronic effects:

$$V_{AB} = \frac{2\varepsilon_0}{\bar{\varepsilon} r}\left[1 - \frac{\sum_{i=e,h} \exp(-\beta_i a_B r)}{2}\right] - \frac{2\varepsilon_0}{\varepsilon_\infty r} + \sum_{i=e,h} \frac{\beta_i a_B r}{\bar{\varepsilon}} \frac{\exp(-\beta_i a_B r)}{1 + \alpha_i/12 + \alpha_i/(4 + \alpha_i/3)}\,, \tag{4.3}$$

where $r = \mathbf{r}_{eh} = |\mathbf{r}_e - \mathbf{r}_h|$, $\beta_i a_B = \left(\frac{m_i}{m_e}\frac{\hbar\omega}{Ry}\right)^{1/2}$, $\alpha_i = \frac{\varepsilon_0}{\bar{\varepsilon}}\frac{R_y}{\hbar\omega}\beta_i a_B$ and $\frac{1}{\bar{\varepsilon}} = \frac{1}{\varepsilon_\infty} - \frac{1}{\varepsilon_0}$. Here ε_∞ and ω denote the high dielectric constant and the longitudinal optical (LO) phonon frequency. In Ref. [57, 61] it has been shown that this potential provides an accurate description of the polaronic effects in narrow QWs, whilst it only considers the interaction with the bulk LO-phonons. In what follows we will use the Aldrich-Bajaj potential in order to describe the exciton-phonon interaction in QWWs.

The solution of the Hamiltonian (4.1) is sought in the form:

$$\Psi(\mathbf{r}_e,\mathbf{r}_h)=f_e(\mathbf{r}_e)f_h(\mathbf{r}_h)\Phi(r), \tag{4.4}$$

where $f_e(\mathbf{r}_e)$ and $f_h(\mathbf{r}_h)$ are the ground-state eigenfunctions of the electron polaron and hole polaron Hamiltonians given in Eq. (2), whereas $\Phi(r)$ is a variational function that describes the intrinsic properties of the exciton bound state. The ground-state energy of the exciton is found by minimizing the following functional $F[\Phi]=\langle f_e f_h\Phi|H_e+H_h+V_{ex}-E_{ex}|f_e f_h\Phi\rangle$. As explained in Ref. [30, 63] after some algebraic manipulations we can obtain the following variational problem:

$$F[\Phi]=\int_0^\infty\left\{J_0(r)\left[(\eta_e+\eta_h)\left(\frac{d\Phi(r)}{dr}\right)^2+(E_e+E_h-E_{ex}-V_{ex})\Phi^2(r)\right]\right\}dr, \tag{4.5}$$

where

$$J_0(r)=\int d\mathbf{r}_e\int f_e^2(\mathbf{r}_e)f_h^2(\mathbf{r}_h)\delta(|\mathbf{r}_e-\mathbf{r}_h|-r)d\mathbf{r}_h. \tag{4.6}$$

The minimization of the functional (5) yields the Euler-Lagrange equation:

$$-\frac{\eta_e+\eta_h}{J_0(r)}\frac{d}{dr}J_0(r)\frac{d\Phi(r)}{dr}-V_{ex}\Phi(r)=\left[E_{ex}-(E_e+E_h)\right]\Phi(r). \tag{4.7}$$

The binding energy of the exciton, $E_b=E_e+E_h-E_{ex}$, is then obtained by solving Eq. (4.7) using the trigonometric sweep method [48]. Note that this differential equation for the correlation function resembles the wave equation for an hydrogenic-like atom in an isotropic effective space with non-fixed fractional dimension. Such a dimension depends on the electron-ion separation and can be calculated by using the Mandelbrot‘s formula that relates its value to the volume element, Jacobian $J_0(r)$, in the fractional-dimensional space [29-30].

In general, in order to find the Jacobian from the relation (6) one should calculate integrals of the fifth order, however, the order of the integrals can be reduced to two for systems with axial symmetry. Thus after some algebraic manipulations the following explicit expressions of the Jacobian $J_0(r)$ for QWs and QWWs are obtained:

$$J_0(r) = 2\pi r \int_{-\infty}^{\infty} f_e^2(z_e)\,dz_e \int_{-r}^{r} f_h^2(z_e + z)\,dz\,; \tag{4.8}$$

$$J_0(r) = 4\pi r \int_{0}^{\infty} f_e^2(\rho_e)\,\rho_e\,d\rho_e \int_{\max\{0,\rho_e - r\}}^{\rho_e + r} K\left(\frac{a}{b}\right)\frac{f_h^2(\rho_h)\,\rho_h}{b}\,d\rho_h\,, \tag{4.9}$$

where $f_e(z_e)$, $f_h(z_h)$ and $f_e(\rho_e)$, $f_h(\rho_h)$ are the ground state wave functions of the electron polaron and hole polaron in QW and cylindrical QWW respectively. In Eq. (4.9) $K(x)$ is the complete elliptic integral of first kind, while $a = \min\left\{4\rho_e\rho_h, \sqrt{r^2 - (\rho_e - \rho_h)^2}\right\}$ and $b = \max\left\{4\rho_e\rho_h, \sqrt{r^2 - (\rho_e - \rho_h)^2}\right\}$.

4.3 RESULTS AND DISCUSSION

To check the accuracy of our method we first calculate the ground state binding energy of excitons in GaAs/$Ga_{0.7}Al_{0.3}As$ and ZnSe/$Zn_{0.69}Cd_{0.31}Se$ QWs for two models of the electron-hole interaction, the Coulomb V_c and Aldrich-Bajaj V_{AB} potentials. The values of the physical parameters used are listed in Table 1.

Table 1. Physical parameters for the GaAs/$Ga_{0.7}Al_{0.3}As$ and ZnSe/$Zn_{0.69}Cd_{0.31}Se$ heterostructures.

Structure	m_e/m_0	γ_1	γ_2	ε_0	ε_∞	$\hbar\omega(meV)$	$V_e(meV)$	$V_h(meV)$
GaAs/GaAlAs	0.067	6.93	2.15	12.5	10.9	35.2	228	152
ZnZe/ZnCdSe								
a	0.148	2.45	0.61	8.7	5.73	31.7	230	115
b	0.160	4.30	1.14					

Values have been taken from Ref. [57, 61]; (a) and (b) correspond to mass parameters determined by resonant Raman scattering [64] and Brillouin scattering [65] respectively.

In Fig. 4.1, the binding energy, E_b, of the heavy–hole exciton is plotted as a function of the well width. It can be seen that the enhancement of the exciton binding energy due to the interaction with the phonon-field in GaAs/GaAlAs is rather small because of its weak ionic structure. On the contrary, the polaronic effect in ZnSe/ZnCdSe is considerable due to the fact that this system is a highly polar heterostructure. For the GaAs/GaAlAs we compare our results (curves) with those from Ref. 57 (symbols) and we find that the discrepancy between them is not superior to 1%. However, we obtain slightly larger binding energies because in our procedure we do not just use variational parameters, instead we use an exciton correlation function which is variational itself, as a consequence we have a greater freedom and we obtain binding energies with a higher accuracy [29, 30]. For ZnSe/ZnCdSe a comparison with theoretical and experimental data from Ref. 61 (symbols) is made. The exciton binding energies, derived through magneto-absorption measurements in quantum wells with widths of 5 and 4 nm, lie between the curves corresponding to theoretical calculations with two different sets of Luttinger parameters (solid lines), whereas the curves without including exciton-phonon interaction (dashed lines) lie below the experimental data. This confirms that the polaronic coupling must be taken into

account in determining the excitonic properties of highly polar QWs. It also shows that the result is sensitive to the Luttinger parameter that should therefore be chosen carefully.

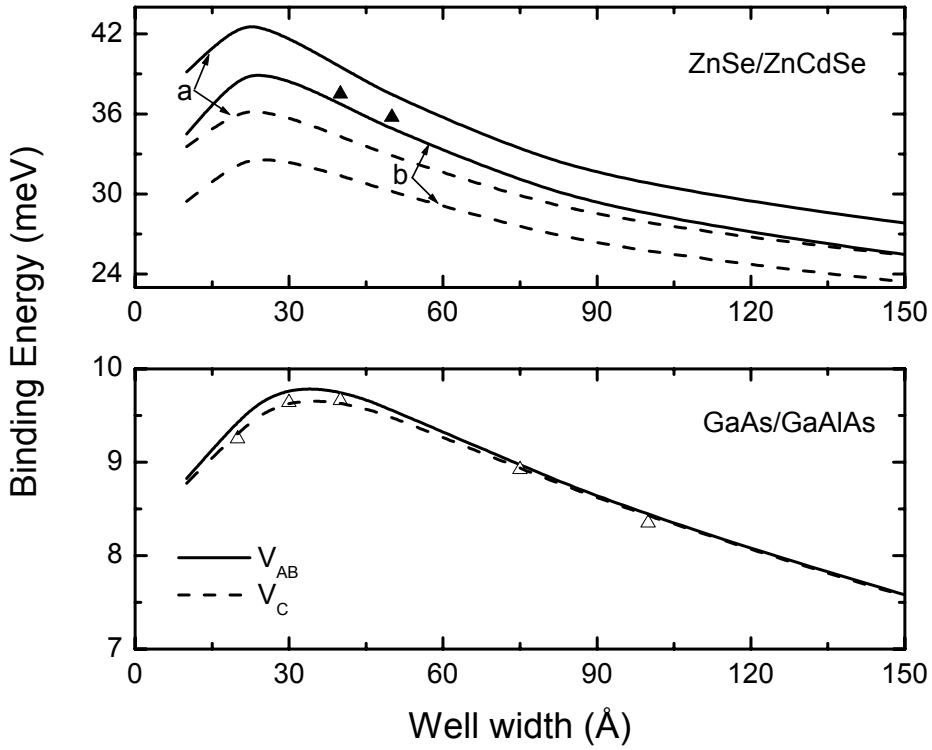

Figure 4.1 Exciton binding energies as a function of the well width for ZnSe/$Zn_{0.69}Cd_{0.31}Se$ (top) and GaAs/$Ga_{0.7}Al_{0.3}As$ (bottom) quantum wells. Solid curves correspond to values obtained by using the Aldrich and Bajaj V_{AB} potential for exciton-phonon interaction and dashed curves to those with Coulomb potential V_C. In the upper plot, a and b denote results as obtained with Luttinger parameters derived by Hölscher et al., and Sermage and Fishman [64 65] respectively. Open triangles correspond to theoretical calculations from Ref. [57] and solid triangles to experimental data from Ref. [61].

Next we study the influence of the LO phonon-field on the binding energies of an exciton in a cylindrical wire both for the GaAs/GaAlAs and ZnSe/ZnCdSe heterostructures. The corresponding results are displayed in Fig. 4.2 where the exciton binding energy as a function of the wire radius is plotted. We compare our results for GaAs/$Ga_{0.7}Al_{0.3}As$ with those of Ref. 8 and we can see that a very good agreement is reached. As expected the enhancement of the binding energy due to the exciton-phonon interaction is larger for the

ZnSe/ZnCdSe structure. By comparison with Fig. 4.1 it can be seen that this effect is stronger for QWWs than for QWs. For instance, for narrow GaAs/GaAlAs QW the values calculated by using the Aldrich-Bajaj interaction are about 1.2% larger than those obtained assuming the simple Coulomb interaction whereas for QWWs the difference between the two set of results for small wire radii is of the order of 2.5%. Furthermore, for ZnSe the enhancement is about 18% in QWs whereas in QWWs is approximately of 25%.

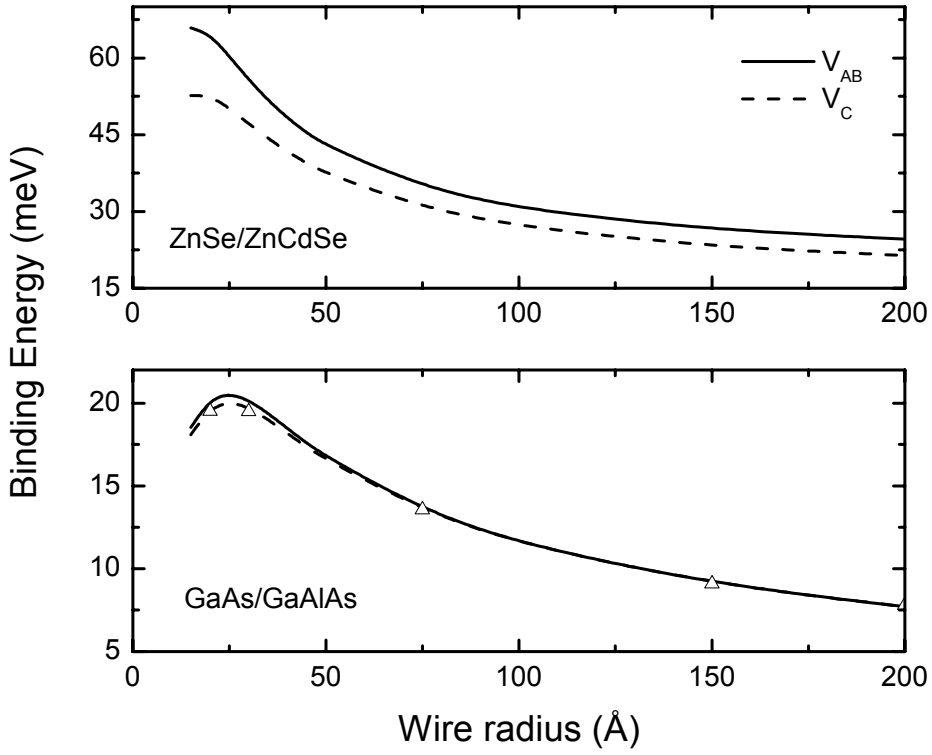

Figure 4.2 Exciton binding energies as a function of wire radius for ZnSe/$Zn_{0.69}Cd_{0.31}Se$ (top) and GaAs/$Ga_{0.7}Al_{0.3}As$ (bottom) quantum wells wires. Solid curves correspond to values obtained by using the Aldrich and Bajaj V_{AB} potential for exciton-phonon interaction and dashed curves to those with Coulomb potential V_C. Open triangles correspond to theoretical calculations from Ref. [8].

It is also important to note that for heterostructures with weak ionic structure the polaronic effect on the binding energy exciton is only appreciable for narrow wells and wires. To understand this result one should take into account that the exciton-phonon interaction

enhances the electron and hole effective masses (polaron mass) and diminishes the electrostatic screening. Both of these effects give rise to the enhancement of the exciton binding energy. As either the well or the wire is narrow, the exciton is more confined and therefore in this region the decrease of the screening produces an increase of the exciton binding energy which is appreciable for both materials, but it is more important in ZnSe because of its lower dielectric constant. On the other hand, the effect of the polaron mass on the exciton binding energy is more important as the size of the heterostructure is larger than the free exciton size. In this range the exciton binding energy is roughly given by the exciton Rydberg. It is clear that a larger polaron mass, increases the exciton Rydberg and as a consequence the exciton binding energy. The mass increase due to polaronic effect is approximately 1.01 for GaAs and 1.10 for ZnSe which explains the finding of negligible polaron effect in wider GaAs/GaAlAs wells and wires in contrast to what happens in ZnSe/ZnCdSe.

In Fig. 4.3 we present the ground state binding energy of the heavy-hole excitons in ZnSe/$Zn_{0.69}Cd_{0.31}Se$ quantum-well wires for different shapes of the confinement potential. The polaronic effects can be explained as done in Fig. 4.1 and Fig. 4.2. Notice that in this case the increase of the binding energy is almost independent from the shape of the potential. However, a different dependence of the binding energy on the wire radius is observed for different potential shape. Comparing the two curves for the square-well and the parabolic potentials (both with the same finite barrier height) one can see that for large radii the latter always has the larger binding energy, this is due to the fact that the effective confinement is stronger for the parabolic potential. As the wire radius decreases the exciton level is pushed out and the exciton wave function starts leaking steadily into the

barriers and for a critical wire radius the 3D character of the exciton wave function is restored. On the contrary, when a square-well confinement is present in this range of wire's widths the exciton is still confined, and the leakage of the exciton wave function occurs at a smaller wire radius.

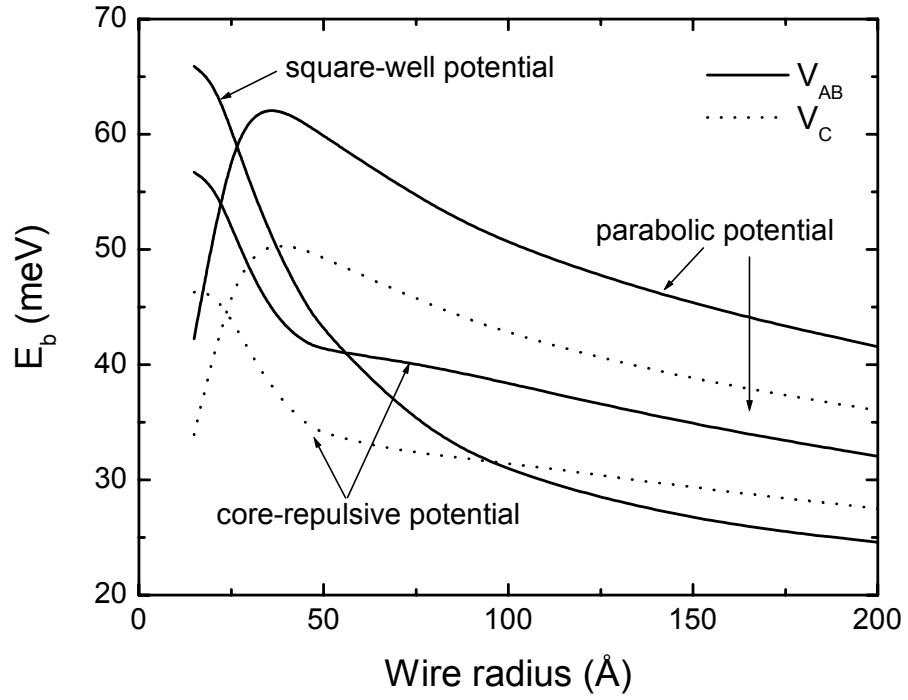

Figure 4.3 Binding energies for exciton in $ZnSe/Zn_{0.69}Cd_{0.31}Se$ quantum wires as a function of the heterostructure sizes and for different confinement potential shapes. Solid curves correspond to values obtained by using the Aldrich and Bajaj V_{AB} potential for exciton-phonon interaction and dotted curves to those with Coulomb potential V_C.

Next we consider the case of a nanotube which is modeled by a quantum wire with repulsive core of internal radius $R_i = 0.5R_e$ and height barrier $V_i = V_e$. The corresponding results are compared with those obtained for the wire ($V_i = 0$) with square-well potential. It can be observed in Fig. 4.3 that the square-well potential gives lower binding energies than the nanotube potential for larger radii, i.e. larger than 60 Å, the opposite happens in the small radii region. This is due to the fact that for large values of the outer radius the

exciton is mostly located within the "ring" of the nanotube and it undergoes stronger confinement compared with the wire. As a result, the exciton binding energy is enhanced as the thickness of such a "ring" is decreased up to a value comparable to the exciton radius. On the contrary, as the thickness of the ring is smaller than the exciton radius and the core size (R_i) is comparable to the exciton size, the electron and hole tend to be located at opposite sides of the repulsive core increasing their separation, which diminishes the binding energy. As a consequence, the exciton binding energies for small wire radius in nanotubes are lower than those in quantum wire and therefore the crossover of the corresponding curves in Fig. 4.3 is observed.

To sum up, we have proposed an unified simple method for calculating the ground state binding energy of the excitons in quantum-well heterostructures based on ionic semiconductors. We take into account the exciton-phonon interaction by using the effective potential derived by Aldrich and Bajaj. We found that polaronic effects are stronger in quantum wires than in quantum wells and we expect that for quantum dots those should be stronger. Our method allows us to study different potential shapes in different heterostructures and as an example a nanotube model was considered. We found that the excitons confinement is stronger in nanotubes if the wire radius is larger than 60 Å and is stronger in the wires if the radius is smaller than 60 Å.

5. HOLE MASS ANISOTROPY AND MAGNETIC FIELD EFFECTS

5.1 THEORETICAL MODEL

In this part of the thesis we extend the method developed previously to study the ground state on an exciton in different heterostructures for a model that takes into account the hole mass anisotropy. We also consider here that the material parameters are uniform throughout the heterostructures. In this case, by using an appropriate scaling for energy and length units the Hamiltonian (2.1) can be rewritten as:

$$H(\mathbf{r}_e,\mathbf{r}_h)=H_0(\mathbf{r}_e,\mathbf{r}_h)-\frac{2}{r_{eh}};\quad H_0(\mathbf{r}_e,\mathbf{r}_h)=-\sum_{i,k=1}^{3}\eta^{e}_{ik}\frac{\partial^2}{\partial x_{ie}\partial x_{ke}}-\sum_{i,k=1}^{3}\eta^{h}_{ik}\frac{\partial^2}{\partial x_{ih}\partial x_{kh}}+U(\mathbf{r}_e,\mathbf{r}_h), \quad (5.1)$$

where $H_0(\mathbf{r}_e,\mathbf{r}_h)$ describes the free motion of the electron and hole confined in the heterostructure, $\mathbf{r}_e=\{x_{1e},x_{2e},x_{3e}\}$ and $\mathbf{r}_h=\{x_{1h},x_{2h},x_{3h}\}$ are the electron and hole position vectors, $U(\mathbf{r}_e,\mathbf{r}_h)$ is a perturbation due to the confinement and the external fields, while $-2/r_{eh}$ and $r_{eh}=|\mathbf{r}_e-\mathbf{r}_h|$ are the energy of the electron-hole interaction and the electron-hole separation, respectively. All lengths are scaled in terms of the electron Bohr radius $\mathrm{a}_o^*=\varepsilon\hbar^2/m_e^*e^2$ and all energies in electron effective Rydberg $R_y^*=e^2/2\varepsilon a_0^*$. Here the coefficients η^e_{ik} and η^h_{ik} describe the relative values and the anisotropy of the electron and hole effective masses. Neglecting the valence band mixing, we have that η^e_{ik} is an identity matrix while η^h_{ik} is a diagonal matrix with elements $\eta_\perp=m_e^*/m_\perp^*$ (in-plane direction) and

$\eta_z = m_e^* / m_z^*$ (z-direction) with $m_\perp^*$ and m_z^* being the effective masses of the hole in the x-y plane and in z-direction respectively.

We assume that the Hamiltonian H_0 for free electron-hole pair is separable and that its solution for the ground state is obtained by solving the eigenvalue problem:

$$H_0(\mathbf{r}_e, \mathbf{r}_h) f_0(\mathbf{r}_e, \mathbf{r}_h) = E_0 f_0(\mathbf{r}_e, \mathbf{r}_h), \tag{5.2}$$

For exciton we solve the Schrödinger equation

$$H(\mathbf{r}_e, \mathbf{r}_h) \Psi(\mathbf{r}_e, \mathbf{r}_h) = E_{ex} \Psi(\mathbf{r}_e, \mathbf{r}_h), \tag{5.3}$$

where E_{ex} is the exciton total energy. Its solution also sought in the form:

$$\Psi(\mathbf{r}_e, \mathbf{r}_h) = f_0(\mathbf{r}_e, \mathbf{r}_h) \Phi(r_{eh}), \tag{5.4}$$

with $\Phi(r_{eh})$ being a variational function that describes the intrinsic properties of the exciton and depends only on the electron-hole separation. The ground state energy of the exciton is calculated by minimizing the functional (2.6). Thus, starting from the Schrödinger variational principle we formulate the problem for exciton in heterostructure a variational one of the following functional:

$$F[\Phi] = \int_0^\infty \left\{ J_1(r) \left[\frac{d\Phi(r)}{dr} \right]^2 + \left[E_0 - E_{ex} - \frac{2\tau}{r} \right] J_0(r) \Phi^2(r) \right\} dr \to \min, \tag{5.5}$$

where $E_0 = E_e + E_h$ is the ground state energy of the uncoupled electron-hole pair and

$$J_0(r) = \int d\mathbf{r}_e \int f_0^2(\mathbf{r}_e, \mathbf{r}_h) \delta(r_{eh} - r) d\mathbf{r}_h; \tag{5.6}$$

$$J_1(r) = \int d\mathbf{r}_e \int \sum_{i,k=1}^{3} \frac{\left(\eta_{ik}^{e} + \eta_{ik}^{h}\right)(x_{ie} - x_{ih})(x_{ke} - x_{kh})}{r_{eh}^2} f_0^2(\mathbf{r}_e, \mathbf{r}_h) \delta(r_{eh} - r) d\mathbf{r}_h. \tag{5.7}$$

The minimization of the functional (5.5) with respect to Φ and its first derivative yields the

One-dimensional Euler-Lagrange equation:

$$-\frac{1}{J_0(r)}\frac{d}{dr}J_1(r)\frac{d\Phi(r)}{dr}-\frac{2}{r}\Phi(r)=\left[E_{ex}-E_0\right]\Phi(r). \tag{5.8}$$

Thus, the exciton binding energy $E_b = E_0 - E_{ex}$ can be obtained as the functions J_0 and J_1 are calculated.

5.2 EXCITON IN QUANTUM WELLS AND QUANTUM-WELL WIRES

We consider an exciton in a GaAs-(Ga, Al)As heterostructure, either QW or QWW, under a uniform magnetic field applied along the *z*-axis. Choosing the symmetric gauge for the magnetic field $\mathbf{A}_e = \mathbf{B}\times(\mathbf{r}_e - \mathbf{r}_h)/2$ and $\mathbf{A}_h = \mathbf{B}\times(\mathbf{r}_h - \mathbf{r}_e)/2$ for electron and hole respectively and neglecting the center-of-mass motion in *x*-*y* plane, the Hamiltonian (5.1) for an exciton in QW can be written in cylindrical coordinates as [7]:

$$H_0(\mathbf{r}_e,\mathbf{r}_h)=-\frac{\partial^2}{\partial z_e^2}-\eta_z\frac{\partial^2}{\partial z_h^2}-(1+\eta_\perp)\frac{1}{\rho}\frac{\partial}{\partial\rho}\rho\frac{\partial}{\partial\rho}+U(\mathbf{r}_e,\mathbf{r}_h); \tag{5.9}$$

$$U(\mathbf{r}_e,\mathbf{r}_h)=V_e(z_e)+V_h(z_h)+\frac{(1+\eta_\perp)\gamma^2\rho^2}{4}, \tag{5.10}$$

where $V_e(z_e)$ and $V_h(z_h)$ are the corresponding confinement potential for the electron and hole respectively, $\rho=\sqrt{(x_e-x_h)^2+(y_e-y_h)^2}$ is the in-plane distance between electron and hole while $\gamma = e\hbar B/2m_e^* cR_y^*$ is the Landau level expressed in Ry^*.

The solution of the Hamiltonian (5.2) is found to be:

$$f_0(\mathbf{r}_e,\mathbf{r}_h)=f_e(z_e)f_h(z_h)\exp\left(-\gamma\rho^2/4\right);\quad E_0=E_e+E_h+(1+\eta_\perp)\gamma\,, \tag{5.11}$$

where $f_e(z_e)$ and $f_h(z_h)$ are solutions of the one-dimensional equations

$$-\eta_i\frac{\partial^2 f_i(z_e)}{\partial z_e^2}+V_e(z_e)f_i(z_e)=E_i f_i(z_e);\quad (i=e,h), \tag{5.12}$$

with E_e and E_h being the lowest energies of the electron and hole in the QW respectively, and $\eta_e=1$ while $\eta_h=\eta_z$. Substituting the wave function (5.11) in equations (5.6) and (5.7) after integrating over the Euler angles we obtain the Jacobians:

$$J_i(r)=2\pi r\int_{-\infty}^{\infty}f_e^2(z_e)dz_e\int_{-r}^{r}e^{-\gamma\left(r^2-z^2\right)/2}f_h^2(z_e+z)R_i(z,r)dz;\quad i=0,1 \tag{5.13}$$

with

$$R_0(z,r)=1;\qquad R_1(z,r)=1+\eta_\perp+(\eta_z-\eta_\perp)\frac{z^2}{r^2}\,. \tag{5.14}$$

For an exciton in QWW, we assume that the wire is sufficiently long, so that the motion along wire axis has translational symmetry and therefore the confinement potential depends only on the in-plane radial coordinate. The Hamiltonian (5.1) can then be written in cylindrical coordinates as:

$$H_0(\mathbf{r}_e,\mathbf{r}_h)=-\frac{1}{\rho_e}\frac{\partial}{\partial\rho_e}\rho_e\frac{\partial}{\partial\rho_e}-\eta_\perp\frac{1}{\rho_h}\frac{\partial}{\partial\rho_h}\rho_h\frac{\partial}{\partial\rho_h}+U(\mathbf{r}_e,\mathbf{r}_h); \tag{5.15}$$

$$U(\mathbf{r}_e,\mathbf{r}_h)=V_e(\rho_e)+\frac{\gamma^2\rho_e^2}{4}+V_h(\rho_h)+\frac{\eta_\perp\gamma^2\rho_h^2}{4}, \tag{5.16}$$

with $V_e(\rho_e)$ and $V_h(\rho_h)$ being the potentials for the electron and hole in the QWW. The solution of the eigenvalue problem (5.2) is found to be

$$f_0(\mathbf{r}_e,\mathbf{r}_h)=f_e(\rho_e)f_h(\rho_h);\quad E_0=E_e+E_h, \tag{5.17}$$

where $f_e(\rho_e)$ and $f_h(\rho_h)$ are solutions of the one-dimensional wave equations:

$$-\frac{\eta_i}{\rho_i}\frac{\partial}{\partial\rho_i}\rho_i\frac{\partial f_i(\rho_i)}{\partial\rho_i}+V_i(\rho_i)f_i(\rho_i)+\frac{\eta_i\gamma^2\rho_i^2}{4}f_i(\rho_i)=E_i f_i(\rho_i);\quad i=e,h \tag{5.18}$$

with E_e and E_h being the lowest energies of the electron and hole in the wire respectively, and $\eta_e=1$ while $\eta_h=\eta_\perp$. As explained above, the Jacobians can be obtain after integrating over the Euler angles and z-coordinates in Eqs. (5.6) and (5.7) as:

$$J_i(r)=4\pi r\int_0^\infty f_e^2(\rho_e)\rho_e d\rho_e\int_{\max\{0,\rho_e-r\}}^{\rho_e+r}f_h^2(\rho_h)R_i(\rho_e,\rho_h,r)\rho_h d\rho_h;\quad i=0,1 \tag{5.19}$$

$$R_0(\rho_e,\rho_h,r)=G_0(\rho_e,\rho_h,r); \tag{5.20}$$

$$R_1(\rho_e,\rho_h,r)=(1+\eta_\perp)G_0(\rho_e,\rho_h,r)+\frac{\eta_z-\eta_\perp}{r^2}G_A(\rho_e,\rho_h,r), \tag{5.21}$$

where $G_0(\rho_e,\rho_h,r)=K(b/a)/a$ as $r>\rho_e+\rho_h$; $G_0(\rho_e,\rho_h,r)=K(a/b)/b$ as $r<\rho_e+\rho_h$; $G_A(\rho_e,\rho_h,r)=aE(b/a)$ as $r>\rho_e+\rho_h$; and $G_A(\rho_e,\rho_h,r)=bE(a/b)$ as $r<\rho_e+\rho_h$, with $a=\sqrt{r^2-(\rho_e-\rho_h)^2}$; $b=\sqrt{4\rho_e\rho_h}$ and $K(k)$, $E(k)$ being the complete elliptic integrals of the first and second kind, respectively.

In our calculations we use the material parameters pertaining to GaAs $\varepsilon=12.53$, $m_e^*=0.067m_0$ with m_0 been the bare electron mass. For the light-hole mass are $m_z^*=0.08m_0$ and $m_\perp^*=0.21m_0$, while for the heavy-hole $m_z^*=0.45m_0$ and $m_\perp^*=0.10m_0$. The values of the parameters η_z and $\eta_\perp$ for these masses are 0.84 and 0.32 for the light-hole exciton, and 0.149 and 0.67 for the heavy-hole exciton.

In order to check the accuracy of the method, we first calculate the exciton binding energy in GaAs/$Ga_{0.7}Al_{0.3}As$ QW and QWW. In Fig. 5.1 and Fig. 5.2 we display the exciton binding energies for heavy-hole, $E_{1s}(h)$, (solid lines) and for light-hole, $E_{1s}(l)$, (dashed lines) as function of the well width. Our results are compared with those from Refs. 6 and 7 (open circles).

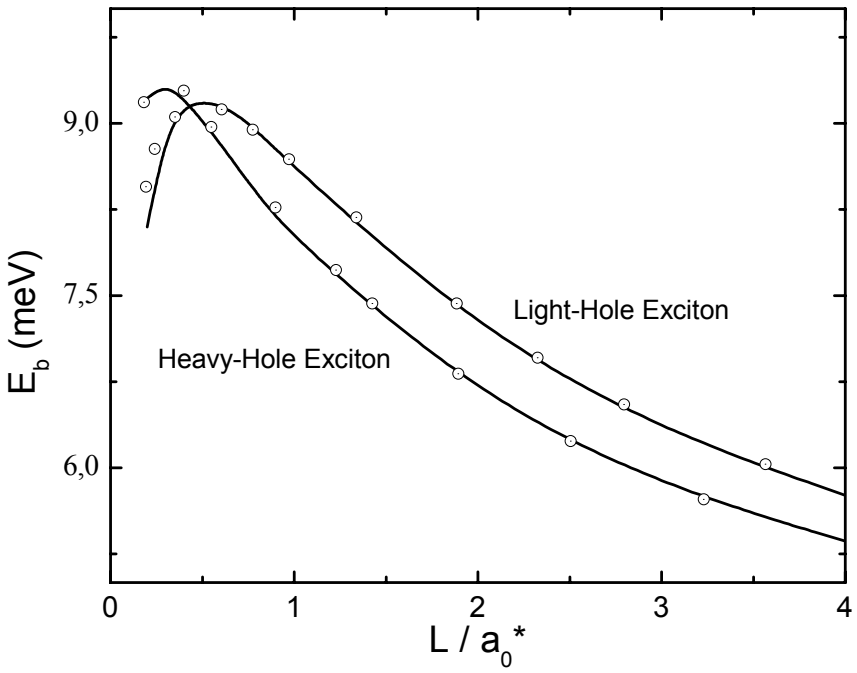

Figure 5.1 The light- and heavy-hole exciton binding energies as a function of the GaAs/$Ga_{0.7}Al_{0.3}As$ QW width. Open circles correspond to calculations from Ref. 6

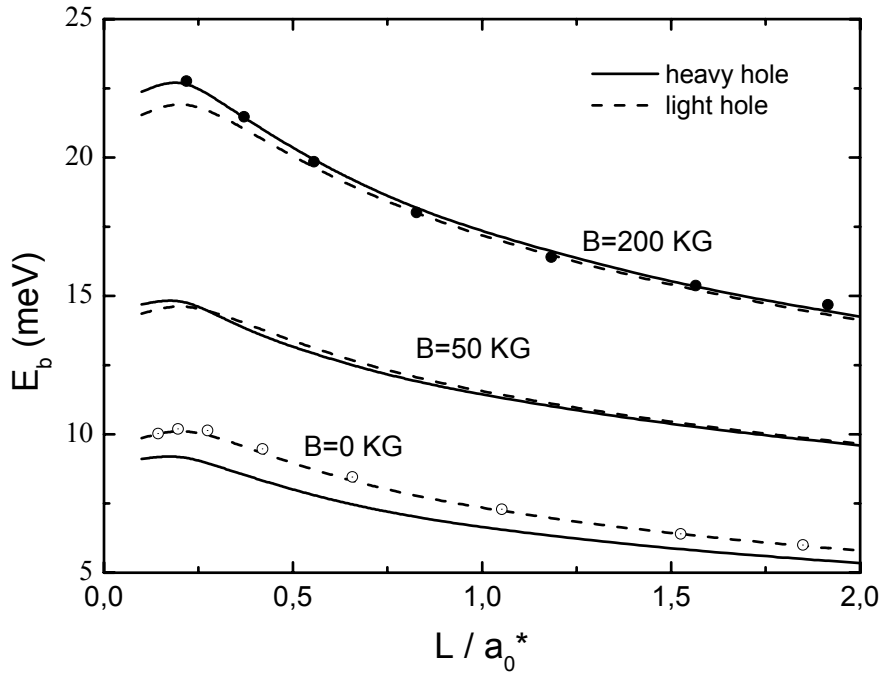

Figure 5.2 The light- and heavy-hole exciton binding energies as a function of the GaAs/$Ga_{0.7}Al_{0.3}As$ QW width for different magnetic field strengths. Open circles correspond to calculations from Ref. 7

In both cases we intentionally choose the material parameters from corresponding references and we find an excellent concordance between the two sets of results for different well widths and magnetic field strengths. As it is seen from the figures the binding energies of the nearly free light-hole exciton (in the limit of large QWs widths and zero-magnetic field) is slightly larger than the corresponding energies for the heavy-hole exciton. The opposite happens when the confinement is strong (the limits of small QWs widths or large magnetic field). This effect was established in Ref. 6 for the case of a structural confinement and it was explained on the base of the anisotropic Kohn-Luttinger model for which the reduced effective mass of the light-hole exciton in the *x*-*y* plane is larger than that for heavy-hole exciton. A similar explanation is also valid for the case of a confinement produced by strong magnetic fields.

Figure 5.3 shows the heavy-hole exciton binding energy as a function of the wire radius for different magnetic fields. Although the isotropic hole mass approximation used in Ref. 8 is applicable only for small electron-hole separations, an excellent concordance between the two sets of results is observed in Fig. 5.3 for all wire radii in the limit of zero-magnetic field.

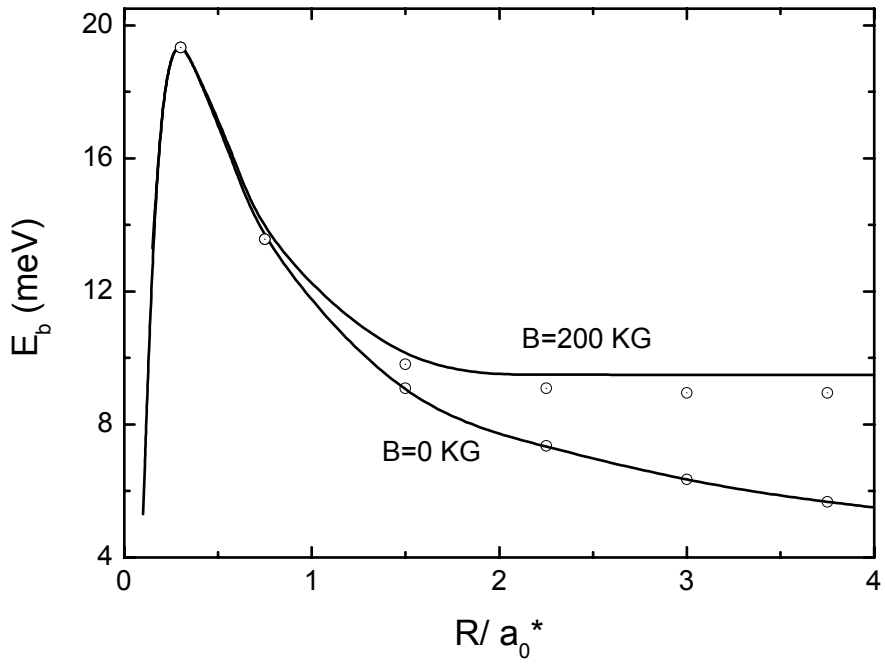

Figure 5.3 Heavy-hole exciton binding energy as a function of the wire radius with and without magnetic field. Our results (solid lines) are compared with theoretical data from Ref. 8 (open circles)

Also it is seen that in the presence of magnetic field (B = 200 KG), for wire radii larger than electron effective Bohr radius, our results are slightly higher than those from Ref. 8. We attribute this small discrepancy to the additional lateral confinement produced by the strong magnetic field that enlarges the effect of anisotropy. In this case, the motion of the particles due to the strong in-plane confinement is almost quasi-one-dimensional and it is oriented along the wire axis. The heavy-hole effective mass in this direction is higher than its value in the *x*-*y* plane and therefore the exciton effective Rydberg (a measure of the

exciton binding energy) for anisotropic model is a slightly greater than for the isotropic one.

In figure 5.4 we illustrate the effect of the structural confinement on the conditional probability density for the heavy-hole exciton at zero-magnetic field defined as:

$$P\left(x_e, z_e / x_h = y_h = z_h = y_e = 0\right) = f_e^2\left(x_e\right)\Phi^2\left(\sqrt{x_e^2 + z_e^2}\right). \tag{5.22}$$

This corresponds to the hole and electron locations on the QWW axis and in the *x*-*z* plane, respectively. It is seen that as the QWW radius decreases the probability density becomes more anisotropic, meanwhile the peak of the distribution becomes more pronounced. It should be noted that the distribution contraction in the radial direction, due to the structural confinement is also accompanied by its weak contraction in the *z*-direction.

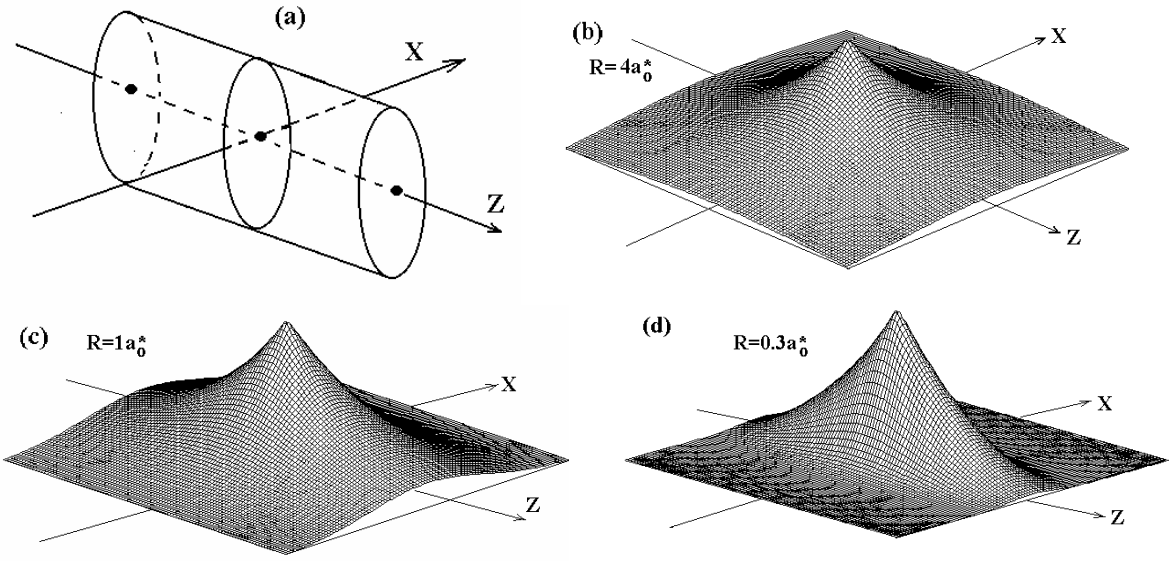

Figure 5.4 Schematic representation of the electron conditional probability density in the x-z plane, for different QWW radii: (b) $R = 4.0a_0^*$, (c) $R = 1.0a_0^*$, (d) $R = 0.3a_0^*$ for the heavy-hole exciton with the fixed hole position at the wire axis.

Figure 5.5 shows the ground state binding energy of exciton as a function of the GaAs-$Ga_{0.7}Al_{0.3}As$ cylindrical QWW radius for different potential shapes: square-well $\left(R_i = 0,\ \ W = 0.01R_e\right)$, soft-edge barrier $\left(R_i = 0,\ \ W = 0.5R_e\right)$, parabolic finite-barrier $\left(R_i = 0,\ \ W = R_e\right)$, and a cylindrical nanotube-like wire with repulsive core $\left(R_i = 0.15R_e,\ \ V_i = V_e,\ \ W = 0.01R_e\right)$.

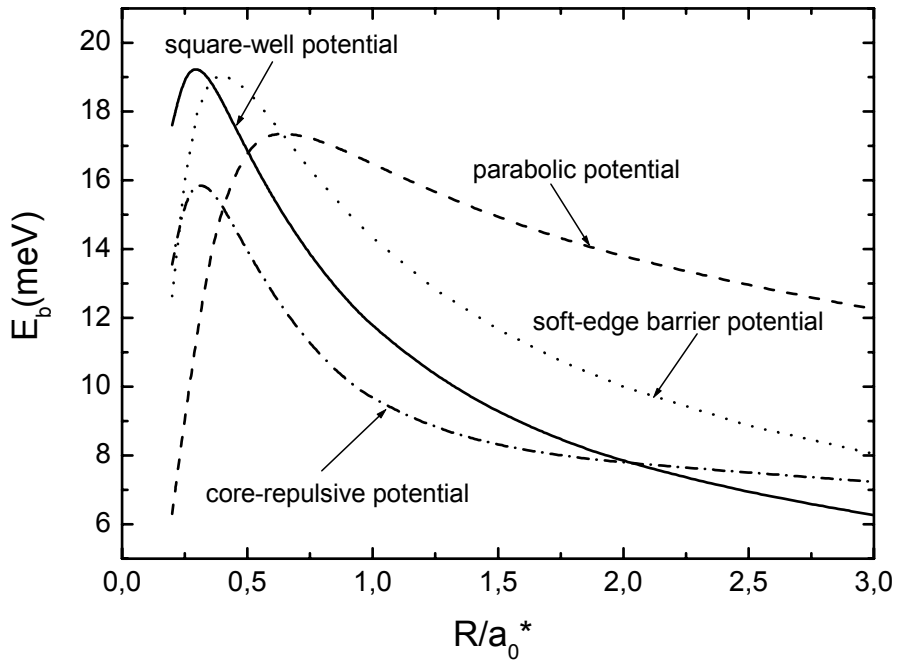

Figure 5.5 Exciton binding energies in GaAs/$Ga_{0.7}Al_{0.3}As$ cylindrical QWWs with different confinement potential shapes as a function of the wire radius.

As one compare the curves for cylindrical QWWs with equal finite barrier height and different potential shapes, square-well (solid line), soft-edge barrier (dotted line) and parabolic (dashed line) potentials one can see that for large and intermediate wire radii the larger the transition region thickness the higher is the binding energy. It is apparent that for intermediate and large values of the QWW radius the parabolic shape gives the largest confinement, followed by the soft-edge barrier, whereas the rectangular potential

corresponds to the smallest confinement. As the wire radius R_e decreases, the exciton binding energy for all potential shapes climbs up until it reaches a maximum. As R_e, further decreases, the exciton wave function leaks into the barrier region and the exciton binding energy begins to fall off rapidly meanwhile the exciton 3D character is restored. It is evident that this leakage of the exciton wave function in QWW with parabolic confinement occurs earlier due to stronger confinement than for the other two types of potential and consequently the maximum of the binding energy for this model is lower than the maxima for the soft-edge-barrier and rectangular potentials. In Fig. 5.5 we also present the results for a nanotube-like structure which is modeled by a quantum wire with repulsive core of internal radius, $R_i = 0.5R_e$ and barrier height $V_i = V_e$ (dashed-dotted line). It is seen that for large QWW radii the exciton binding energies in nanotubes are higher than those in QWWs with square-well potential (solid line) and conversely for small radii. This is due to the fact that for large outer radii, R_e, both electron and hole are mostly located within the "ring" of the nanotube on the same side with respect to the core and the exciton undergoes a stronger confinement than in the wire. As consequence, the exciton binding energy is enhanced as the thickness of such "ring" is decreased up to a value comparable with the exciton radius. On the contrary, as the ring thickness is smaller than the exciton radius and the core size (R_i) is comparable with the exciton size, the electron and the hole tend to be located at opposite sides of the repulsive core, the separation between them increases and the binding energy diminishes. As consequence, the exciton binding energies for small wire radii in nanotubes are lower than those in quantum wire and therefore, the crossover of the corresponding curves in Fig. 5.5 is observed.

5.3 EXCITON IN TWO DIMENSIONAL QUANTUM RING

In this section we apply our method to analyze the effects of the magnetic field and the potential shape on the binding energy of excitons in quantum rings (QRs). We consider a two-dimensional exciton in a ring-shaped $In_xGa_{1-x}As/GaAs$ quantum dot in the presence of a uniform magnetic field oriented along the *z* axis, perpendicular to the plane of the ring. For this model, the wave functions of the free electron and hole in the state of lower energy in the QR are also described by Eqs. (5.17) and (5.18). As the system is essentially two-dimensional the Jacobian anisotropic part in Eq. (5.19) vanishes ($J_1 = 0$), and the integral for the isotropic part $J_0(r)$ becomes of the fourth order. Then, after integrating in the expression (5.19) for the Jacobian over the two angular coordinates one can reduce it to the following integral of second order:

$$J_0(r) = J(r) = 2r\int_0^{\infty} f_e^2(\rho_e)\rho_e d\rho_e \int_{|\rho_e - r|}^{\rho_e + r} \frac{f_h^2(\rho_h)\rho_h d\rho_h}{\sqrt{\left[r^2 - (\rho_e - \rho_h)^2\right]\left[(\rho_e + \rho_h)^2 - r^2\right]}}. \qquad (5.23)$$

Once the Jacobian is calculated the exciton binding energy can then be found from the differential equation (5.8) by using a procedure similar to one described above for QW and QWW.

In our calculation the dielectric constant is assumed to be $\varepsilon = 13$ and the hole in-plane effective mass $m_{\perp}^{*} = 0.25m_0$ [66]. The potential with different shapes in QR is also modeled by Eq. (2.22) with R_i and R_e being the internal and external radii of the ring. By choosing $W = 0.01(R_e - R_i)$ we simulate the almost rectangular potential, $W = 0.2(R_e - R_i)$

QR with the soft-edge barrier potential and $W = 0.5(R_e - R_i)$ QR with the parabolic finite barrier potential. The corresponding barrier heights V_i and V_e are chosen as $0.7\Delta E_g x_{i(e)}$ for the electron and $0.3\Delta E_g x_{i(e)}$ for the hole, being x_i and x_e the concentration of indium in the core and in the barrier, respectively, and $\Delta E_g = 1.11\,eV$ [16] being the band gap difference between GaAs and InAs.

In Fig. 5.6 we plot the binding energy of an exciton confined in QRs with different inner radii and fixed ratio of the barrier heights $V_i/V_e = 0.5$ as a function of the ring width $(R_e - R_i)$ for different values of the magnetic field strength. One can see that in the case of the quantum disk ($R_i = 0$) and QRs with small core radius ($R_i = 1\,nm$) the binding energy climbs up in the narrowing ring until it reaches a maximum and further as the ring width decreases the binding energy begins to fall off sharply. We consider this binding-energy jump as dimensionality instability associated with the restoring of the two-dimensional character of the electron wave function which leaks into to the barrier region when the confinement reaches a critical value (see solid lines in Fig. 5.6 (b) and inset). With increasing the core radius the binding energy dependence on the ring width becomes different (see solid line in Fig. 5.6 (a) and dashed and dotted lines in Fig. 5.6 (b)), the pronounced maximum in the region of small QR widths disappears and the additional shoulder emerges in the region of intermediate QR widths. We associate these shoulders with the effect of the electron wave function spreading in the core region when the exterior barrier approaches to the core. As the QR width decreases, it reaches a critical value when the electron (whose effective mass is less than one of the hole) is pushed upwards from the

ring toward the core region, increasing the electron-hole separation and decreasing the binding energy. The hole undergoes a similar effect of the ejection in the core region for smaller width, as the electron-hole separation decreases and the exciton binding energy begins to grow again.

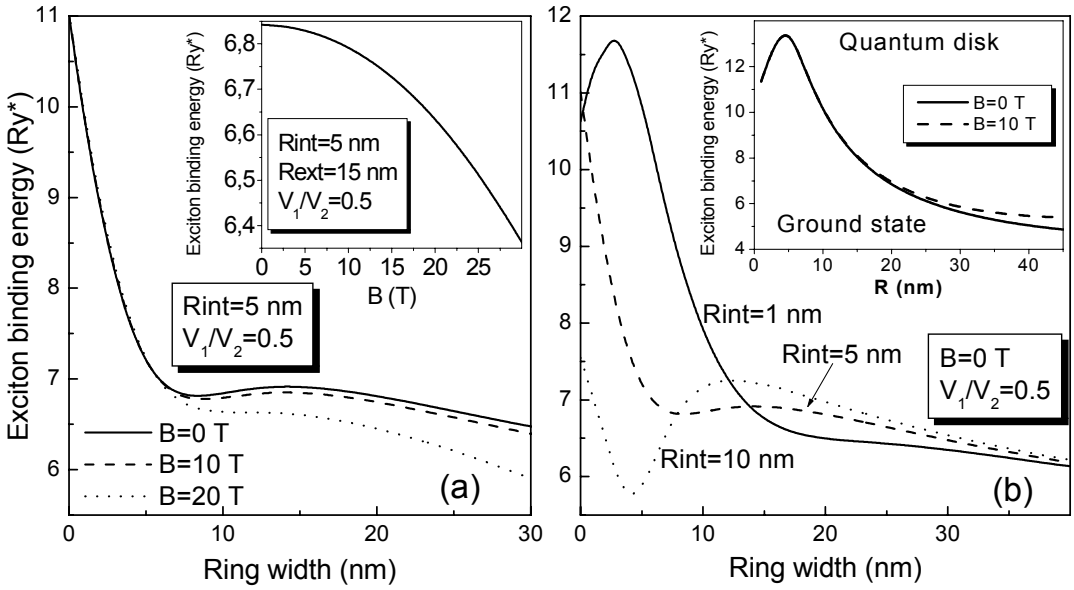

Figure 5.6 Exciton binding energy as a function of the ring width for different values of the magnetic field and core's radius. Inset in (a) shows the binding energy as a function of the magnetic field for a given ring width and in (b) shows the exciton binding energy in a quantum disk as a function of the disk radius.

In the inset in Fig. 5.6 (a) is shown the dependence of the ground state binding energy in QR on the strength of the magnetic field. It is seen that this dependence is different from the similar one for quantum disk, where the binding energy increases in the presence of the magnetic field. In the case of the quantum disk the magnetic field produces additional confinement which increases the probability of location near to the center of the disk of both electron and hole and decreases the electron-hole separation. On the contrary in the case of the QR the magnetic field increases the tunneling into the core region only for the electron whose effective mass is less than the mass of the hole. The effect of the magnetic

field upon the heavier hole is very weak and therefore the hole remains located mostly in the middle of the ring between the interior and the exterior barriers. As result the electron-hole separation in the presence of the magnetic field increases and the exciton binding energy falls.

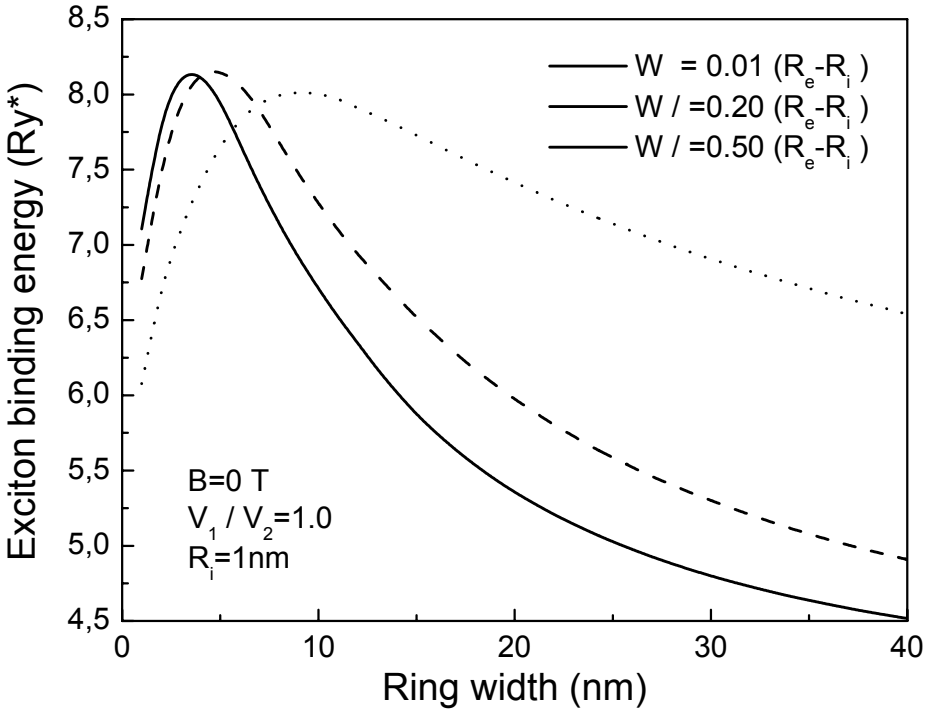

Figure 5.7 Exciton binding energy as a function of the ring width, for three different profiles of the potential barriers.

The effect of the potential shape on the exciton ground state binding energy can be observed in Fig. 5.7 where we show the exciton binding energy as a function of the ring width for three different profiles of the potential barrier, modeled by choosing in the relation (2.22) the parameter *W* equal to 1% (nearly square-well potential), 20% (smooth potential) and 50%(parabolic potential) of the QR width. Our results for rectangular and parabolic potentials are in a good agreement with those of Ref. [21] obtained by using different calculation method. It is seen from the Fig. 5.7 that for large values of the ring

width the parabolic potential (dotted curve) gives the largest binding energy, followed by the (dashed curve), whereas the square-well potential (solid curve) gives the smallest binding energy. On the contrary, when the ring width is small, the effects of the potential shapes on the binding energy are in conversely order, being the square-well potential which presents the largest energy, therefore, a crossover in the corresponding curves in Fig 5.7 is evident.

6. CONCLUSIONS

We have developed a simple and unified method to study the ground state of exciton in semiconductor heterostructures with different potential shapes. We also study the influence of an external magnetic field and the effect of the longitudinal-optical phonon field on the binding energies of exciton in quantum wells and quantum-well wires based on ionic semiconductors. The method was proven to work very well even when the carriers confinement is stronger. Its accuracy was tested by comparison with other sophisticate methods such as the finite difference technique, the stochastic variational method among others.

We demonstrated that when an isotropic model for the hole mass is taken, our method allow us to reduce the problem of exciton in heterostructure to one similar to the hydrogen-like atom in fractional dimensional space where its dimension is related to the anisotropy of the actual semiconductor system. The concept of a *running dimension* is introduced and we show that the dimension is not the same in the hole space, but it depends on the electron-hole distance in the heterostructure which depends on the spatial confinement.

We show that if the confinement potential is neither square-well nor parabolic, an effect on the exciton binding energy appeared. This consist in that the square-well potential produces the stronger confinement for small sizes of the heterostructure but the weakest one for larger sizes of the semiconductor structure. We also considered potential models

for a nanotube-like structure and a double-step heterostructure. In the latter the main fact is that the exciton binding energy reaches two maxima as the exciton is confined with decreasing size of the heterostructure. By controlling its size is possible to obtain two peaks or just one in the curve of the binding energy. In the nanotube case, we found that this produces an intermediate confinement between the rectangular and parabolic potential as the characteristic length of the heterostructure is large.

We also found a novel effect on the exciton binding energy in quantum rings. In comparison to the quantum disk case, the ring gives rise to a shoulder o second peak of the binding energy with decreasing ring width. This effect is similar to that in heterostructures with double-step potentials.

It would be very interesting to extend the method to study the first excited state of an exciton in heterostructures semiconductors, as well as, to consider the effect of the parameter material mismatch.

REFERENCES

1. Zh. I. Alferov, Rev. Mod. Phys. **73**, 767 (2001)
2. D.A. Miller, *In Optical Switching in Low-Dimensional Systems*, edited by H. Hang and Libanyai (Plenum, New York, 1988), pp. 1-8
3. M. Jaros, *Physics and Applications of Semiconductor Microestructure*, (Clarendon Press, Oxford, 1989)
4. M. J. Kelly, *Low-Dimensional Semiconductors*, (Clarendon Press, Oxford, 1995)
5. G. Bastard, E.E. Mendez, L. L. Chang and L. Esaki, Phys. Rev. B **26**, 1974 (1982)
6. R. L. Greene, K.K. Bajaj and D.E. Phelps, Phys. Rev. B **29**,1807(1984)
7. J. Cen and K.K. Bajaj, Phys. Rev. B **50**, 10947 (1994)
8. Gang Li, S. V. Branis and K. K. Bajaj, J. Appl. Phys. **77**, 1097 (1995)
9. S. Le Goff and B. Stébé, Phys. Rev. B **47**, 1383 (1993)
10. T. Garm, J. Phys.: Condens. Matter. **8**, 5725 (1996)
11. J. M. Ferreyra and C. R. Proetto, Phys. Rev. B **57**, 9061 (1998); P. G. Bolcatto and C. R. Proetto, Phys. Rev. B **59**, 12487 (1999)
12. T. Takagahara, Phys. Rev. B **47**, 4569 (1993); **60**, 2638 (1999); **62**, 16840 (2000)
13. R. Winkler, Phys. Rev. B **51**, 14395 (1995).
14. S. Glutsch, F. Bechstedt, W. Wegscheider and F. Schedelbeck, Phys. Rev. B **56**, 4108 (1997)
15. B. Gerlach, J, Wüthoff. M. 0. Dzero and M. A. Smondyrev, Phys. Rev. B **58**, 10568 (1998)

16. B. Szafran, J. Adamowiski and S. Bednarek. J. Phys.: Condens. Mater. **14**, 73 (2002); M. Ciurla, J. Admowski, B. Szafran and S. Bednarek, Physica E **15**, 261 (2002)
17. P. Villamil, C. Beltrán and Nelson Porras-Montenegro, J. Phys.: Condens. Mater. **13**, 4143 (2001)
18. C. Riva, F. M. Peeters and K. Varga, Phys. Rev. B **61**, 13873 (2000)
19. K. L. Janssens, B. Partoens, and F. M. Peeters, Phys. Rev. B **64**, 155324 (2001)
20. K. L. Janssens, B. Partoens, and F. M. Peeters, Phys. Rev. B **66**, 075314 (2002)
21. J. Song and S. E. Ulloa, Phys. Rev. B **63**, 125302 (2001)
22. A.O. Govorov, S. E. Ulloa, K. Karrai and R. J. Warburton, Phys. Rev. B **66**, 081309(R) (2002)
23. Jian-Bai Xia and Shu-Shen Li, Phys. Rev. B **66**, 035311 (2002)
24. R. A. Escorcia, R. Robayo and I. D. Mikhailov, Phys. Stat. Sol. (b) **230**, 431 (2002)
25. X-F. He, Phys. Rev. B **42**, 11751 (1990); B **43**, 2063, (1991)
26. F. H. Stillinger, J. Math. Phys. **18**, 1224 (1977).
27. H. Mathieu, P. Lefebvre and P. Christol, Phys. Rev. **B 46** 4092 (1992); P. Lefebvre, P. Christol and H. Mathieu, Phys. Rev. **B 48** 17308B (1993); P. Lefebvre, P. Christol, H. Mathieu and S. Glutsch, Phys. Rev. **B 52** 5756 (1995)
28. E. Reyes-Gómez, A. Matos-Abiague, C. A. Perdomo-Leiva, M. de Dios-Leyva and L. E. Oliveira, Phys. Rev. B **61**, 13104 (2000); E. Reyes-Gómez, A. Matos-Abiague, M. de Dios-Leyva and L. E. Oliveira, Phys. Stat. Sol. (b) **220**, 71 (2000); E. Reyes-Gómez, C. A. Perdomo-Leiva, L. E. Oliveira, and M. de Dios-Leyva, Physica E **8**, 239 (2000); L. E. Oliveira, C. A. Duque, N. Porras-Montenegro and M. De Dios-Leyva, Physica B **302-303**, 72 (2001)

29. I. D. Mikhailov, F. J. Betancur, R. A. Escorcia and J. Sierra-Ortega, Phys. Stat. Sol. (b) **234**, 590 (2002)
30. I. D. Mikhailov, F. J. Betancur, R. A. Escorcia and J. Sierra-Ortega, Phys. Rev. B **67**, 115317 (2003)
31. N. W. Ashcroft, and N. D. Mermin, *Solid State Physics*, (Saunders College, Philadelpia, 1976)
32. J. C. Phillips, *Bonds and Bands in Semiconductors*, (Academic Press, London, 1973)
33. P. Y. Yu and M. Cardona, *Fundamentals of Semiconductor*: *Physics and Material Properties* (Springer-Verlag, Berlin, 2001)
34. J. S. Blakemore, J. Appl. Phys. **53**, R123 (1982)
35. G. Dresselhaus, A. F. Kip, and C. Kittel, Phys. Rev. B **98**, 368 (1955)
36. G. Bastar, Wave Mechanics Applied to Semiconductor Heterostructures, (Les Éditions de Physique, Les Ulis, 1988)
37. E. O. Kane, *in Handbook on Semiconductors*, *Vol. I*, edited by W. Paul (North-Holland, Amsterdam, 1982)
38. J. M. Luttinger and W. Kohn, Phys. Rev. B **97**, 869 (1955)
39. J. H. Davies, *The Physics of Low-dimensional Semiconductors*, (Cambridge University Press, Cambridge, 1998)
40. C. F. Klingshirn, *Semiconductor Optics*, (Springer-Verlag, Berlin, 1997)
41. J. P. Harbison and R. E. Nahory, *Harnessing the Atom's Light*, (The Scientific American Lybrary, New York, 1998)
42. H. Gislason, W. Langbein and J. M. Hvam, Appl. Phys. Lett. **69**, 3248 (1996)
43. B. P. Zhang *et al*., Materials Science and Engineering B **51**, 224 (1998)
44. M. Grundmann *et al*., Int. J. of Nonlinear Optical Physics and Materials *4*, 99 (1995)

45. P. L. McEuen, Science 278, 1729 (1997)
46. A. C. Jones, and P. O'Brien, *CVD of Compound Semiconductors*: *Precursor Synthesis, Development and Applications* (VCH Weinheim, Cambridge, 1997)
47. B. B. Mandelbrot, *The Fractal Geometry of Nature*, W. H. Freeman (1983).
48. F. J. Betancur, I. D. Mikhailov and L. E. Oliveira, J. Phys. D: Appl. Phys. **31**, 3391 (1998)
49. S. Bednarek, B. Szafran and J. Adamowiski, Phys. Rev. B **64**, 195303 (2001)
50. M. A. Haase, J. Qui, J. M. DePuydt, H. Cheng, Appl. Phys. Lett. **59**, 1272 (1991)
51. W. S. Su, M. H. Ya, Y. S. Chiu, Y. F. Chen, Phys. Rev. B **66**, 113305 (2002)
52. W. Li, W. Sang, J. Min, F. Yu, B. Zhang, K. Wang, Semicond. Sci. Technol. **17**, 155 (2002)
53. P. Redlinski, J. Kossut, Semicond. Sci. Technol. **17**, 237 (2002)
54. G. Q. Hai, F. M. Peeters, J. T. Devreese, Phys. Rev. B **42**, 11063 (1990)
55. M. H. Degani, O. Hipólito, Phys. Rev. B **35**, 9345 (1987)
56. M. Matsura, Phys. Rev. B **37**, 6977 (1988)
57. A. Antonelli, J. Cen, K. K. Bajaj, Semicond. Sci. Technol. **11**, 74 (1996)
58. H. Fröhlich, Adv. Phys. **3**, 6977 (1954)
59. J. Polmann, H. Büttner, Solid State Commun. **17**, 1171 (1975); Phys. Rev. B **16**, 4480 (1977)
60. C. Aldrich, K.K. Bajaj, Solid State Commun. **22**, 157 (1977)
61. A. De Nardis, V. Pellegrini, R. Colombelli, F. Beltrán, L. Vanzetti, A. Franciosi, I. N. Krivorotov, K. K. Bajaj, Phys. Rev. B **61**, 1700 (2000)
62. A. Thilagam, Phys. Rev. B **56**, 9798 (1997)

63. C. Riva, R. A. Escorcia, A. O. Govorov and F. M. Peeters, Phys. Rev. B **69**, 245306 (2004); C. Riva, R. A. Escorcia and F. M. Peeters, Physica E **22**, 550 (2004)
64. H. W. Hölscher, A. Nöthe, Ch. Uihlein, Phys. Rev. B **31**, 2379 (1985)
65. B. Sermage, G. Fishman, Phys. Rev. B **57**, 1749 (1998)
66. M. Grundman, O. Stier and Bimberg, Phys. Rev. B **52**, (1995)

BIBLIOGRAPHY

A. Antonelli, J. Cen, K. K. Bajaj, Semicond. Sci. Technol. **11**, 74 (1996)

A. C. Jones, and P. O'Brien, *CVD of Compound Semiconductors*: *Precursor Synthesis, Development and Applications* (VCH Weinheim, Cambridge, 1997)

A. De Nardis, V. Pellegrini, R. Colombelli, F. Beltrán, L. Vanzetti, A. Franciosi, I. N. Krivorotov, K. K. Bajaj, Phys. Rev. B **61**, 1700 (2000)

A. Thilagam, Phys. Rev. B **56**, 9798 (1997)

A.O. Govorov, S. E. Ulloa, K. Karrai and R. J. Warburton, Phys. Rev. B **66**, 081309(R) (2002)

B. B. Mandelbrot, *The Fractal Geometry of Nature*, W. H. Freeman (1983).

B. Gerlach, J, Wüthoff. M. 0. Dzero and M. A. Smondyrev, Phys. Rev. B **58**, 10568 (1998)

B. P. Zhang *et al*., Materials Science and Engineering B **51**, 224 (1998

B. Sermage, G. Fishman, Phys. Rev. B **57**, 1749 (1998)

B. Szafran, J. Adamowiski and S. Bednarek. J. Phys.: Condens. Mater. **14**, 73 (2002); M. Ciurla, J. Admowski, B. Szafran and S. Bednarek, Physica E **15**, 261 (2002)

C. Aldrich, K.K. Bajaj, Solid State Commun. **22**, 157 (1977)

C. F. Klingshirn, *Semiconductor Optics*, (Springer-Verlag, Berlin, 1997)

C. Riva, F. M. Peeters and K. Varga, Phys. Rev. B **61**, 13873 (2000)

C. Riva, R. A. Escorcia, A. O. Govorov and F. M. Peeters, Phys. Rev. B **69**, 245306 (2004); C. Riva, R. A. Escorcia and F. M. Peeters, Physica E **22**, 550 (2004)

D.A. Miller, *In Optical Switching in Low-Dimensional Systems*, edited by H. Hang and Libanyai (Plenum, New York, 1988), pp. 1-8

E. O. Kane, *in Handbook on Semiconductors*, *Vol. I*, edited by W. Paul (North-Holland, Amsterdam, 1982)

E. Reyes-Gómez, A. Matos-Abiague, C. A. Perdomo-Leiva, M. de Dios-Leyva and L. E. Oliveira, Phys. Rev. B **61**, 13104 (2000); E. Reyes-Gómez, A. Matos-Abiague, M. de Dios-Leyva and L. E. Oliveira, Phys. Stat. Sol. (b) **220**, 71 (2000); E. Reyes-Gómez, C. A. Perdomo-Leiva, L. E. Oliveira, and M. de Dios-Leyva, Physica E **8**, 239 (2000); L. E. Oliveira, C. A. Duque, N. Porras-Montenegro and M. De Dios-Leyva, Physica B **302-303**, 72 (2001)

F. H. Stillinger, J. Math. Phys. **18**, 1224 (1977).

F. J. Betancur, I. D. Mikhailov and L. E. Oliveira, J. Phys. D: Appl. Phys. **31**, 3391 (1998)

G. Bastar, Wave Mechanics Applied to Semiconductor Heterostructures, (Les Éditions de Physique, Les Ulis, 1988)

G. Bastard, E.E. Mendez, L. L. Chang and L. Esaki, Phys. Rev. B **26**, 1974 (1982)

G. Dresselhaus, A. F. Kip, and C. Kittel, Phys. Rev. B **98**, 368 (1955)

G. Q. Hai, F. M. Peeters, J. T. Devreese, Phys. Rev. B **42**, 11063 (1990)

Gang Li, S. V. Branis and K. K. Bajaj, J. Appl. Phys. **77**, 1097 (1995)

H. Fröhlich, Adv. Phys. **3**, 6977 (1954)

H. Gislason, W. Langbein and J. M. Hvam, Appl. Phys. Lett. **69**, 3248 (1996)

H. Mathieu, P. Lefebvre and P. Christol, Phys. Rev. **B 46** 4092 (1992); P. Lefebvre, P. Christol and H. Mathieu, Phys. Rev. **B 48** 17308B (1993); P. Lefebvre, P. Christol, H. Mathieu and S. Glutsch, Phys. Rev. **B 52** 5756 (1995)

H. W. Hölscher, A. Nöthe, Ch. Uihlein, Phys. Rev. B **31**, 2379 (1985)

I. D. Mikhailov, F. J. Betancur, R. A. Escorcia and J. Sierra-Ortega, Phys. Stat. Sol. (b) **234**, 590 (2002)

I. D. Mikhailov, F. J. Betancur, R. A. Escorcia and J. Sierra-Ortega, Phys. Rev. B **67**, 115317 (2003)

J. C. Phillips, *Bonds and Bands in Semiconductors*, (Academic Press, London, 1973)

J. Cen and K.K. Bajaj, Phys. Rev. B **50**, 10947 (1994)

J. H. Davies, *The Physics of Low-dimensional Semiconductors*, (Cambridge University Press, Cambridge, 1998)

J. M. Ferreyra and C. R. Proetto, Phys. Rev. B **57**, 9061 (1998); P. G. Bolcatto and C. R. Proetto, Phys. Rev. B **59**, 12487 (1999)

J. M. Luttinger and W. Kohn, Phys. Rev. B **97**, 869 (1955)

J. P. Harbison and R. E. Nahory, *Harnessing the Atom's Light*, (The Scientific American Lybrary, New York, 1998)

J. Polmann, H. Büttner, Solid State Commun. **17**, 1171 (1975); Phys. Rev. B **16**, 4480 (1977)

J. S. Blakemore, J. Appl. Phys. **53**, R123 (1982)

J. Song and S. E. Ulloa, Phys. Rev. B **63**, 125302 (2001)

Jian-Bai Xia and Shu-Shen Li, Phys. Rev. B **66**, 035311 (2002)

K. L. Janssens, B. Partoens, and F. M. Peeters, Phys. Rev. B **64**, 155324 (2001)

K. L. Janssens, B. Partoens, and F. M. Peeters, Phys. Rev. B **66**, 075314 (2002)

M. A. Haase, J. Qui, J. M. DePuydt, H. Cheng, Appl. Phys. Lett. **59**, 1272 (1991)

M. Grundman, O. Stier and Bimberg, Phys. Rev. B **52**, (1995)

M. Grundmann *et al*., Int. J. of Nonlinear Optical Physics and Materials *4*, 99 (1995)

M. H. Degani, O. Hipólito, Phys. Rev. B **35**, 9345 (1987)

M. J. Kelly, *Low-Dimensional Semiconductors*, (Clarendon Press, Oxford, 1995)

M. Jaros, *Physics and Applications of Semiconductor Microestructure*, (Clarendon Press, Oxford, 1989)

M. Matsura, Phys. Rev. B **37**, 6977 (1988)

N. W. Ashcroft, and N. D. Mermin, *Solid State Physics*, (Saunders College, Philadelpia, 1976)

P. L. McEuen, Science 278, 1729 (1997)

P. Redlinski, J. Kossut, Semicond. Sci. Technol. **17**, 237 (2002)

P. Villamil, C. Beltrán and Nelson Porras-Montenegro, J. Phys.: Condens. Mater. **13**, 4143 (2001)

P. Y. Yu and M. Cardona, *Fundamentals of Semiconductor*: *Physics and Material Properties* (Springer-Verlag, Berlin, 2001)

R. A. Escorcia, R. Robayo and I. D. Mikhailov, Phys. Stat. Sol. (b) **230**, 431 (2002)

R. L. Greene, K.K. Bajaj and D.E. Phelps, Phys. Rev. B **29**,1807(1984)

R. Winkler, Phys. Rev. B **51**, 14395 (1995).

S. Bednarek, B. Szafran and J. Adamowiski, Phys. Rev. B **64**, 195303 (2001)

S. Glutsch, F. Bechstedt, W. Wegscheider and F. Schedelbeck, Phys. Rev. B **56**, 4108 (1997)

S. Le Goff and B. Stébé, Phys. Rev. B **47**, 1383 (1993)

T. Garm, J. Phys.: Condens. Matter. **8**, 5725 (1996)

T. Takagahara, Phys. Rev. B **47**, 4569 (1993); **60**, 2638 (1999); **62**, 16840 (2000)

W. Li, W. Sang, J. Min, F. Yu, B. Zhang, K. Wang, Semicond. Sci. Technol. **17**, 155 (2002)

W. S. Su, M. H. Ya, Y. S. Chiu, Y. F. Chen, Phys. Rev. B **66**, 113305 (2002)

X-F. He, Phys. Rev. B **42**, 11751 (1990); B **43**, 2063, (1991)

Zh. I. Alferov, Rev. Mod. Phys. **73**, 767 (2001)

Appendix A. Publications

R. A. Escorcia, C. Riva, and I. D. Mikhailov, *Polaronic exciton in quantum wells wires and nanotubes* (to be published in Solid. State. Communications 2004)

R. A. Escorcia, J. Sierra-Ortega, I. D. Mikhailov, and F. J. Betancur, *Exciton Fractional Dimension in Semiconductor Heterostructures Arising from Variational Principle*, (to be published in Physica B 2004)

R. A. Escorcia, R. Robayo, and I. D. Mikhailov, *Renormalized Schrödinger Equation for Exciton in Graded Quantum Dot*, Phys. Stat. Sol. (b) **230**, 431 (2002)

F. J. Betancur, F. García, and R. A. Escorcia, *Exciton Binding Energy in Symmetrical Step Quantum Wells*, Rev. Col. Fís. **33**, 152 (2001)

C. Riva, R. A. Escorcia, A. O. Govorov, and F. M. Peeters, *Charged donors in quantum dots: Finite difference and fractional dimensions results*, Phys. Rev. B **69**, 245306 (2004)

C. Riva, R. A. Escorcia, and F. M. Peeters, *Neutral and charged donor in a 3D quantum dot*, Physica E **22**, 550 (2004)

F. J. Betancur, J. Sierra-Ortega, R. A. Escorcia, J. D. González, and I. D. Mikhailov, *Density of impurity states in doped spherical quantum dots*, Physica E **23**, 102 (2004)
I. D. Mikhailov, F. J. Betancur, R. A. Escorcia, and J. Sierra-Ortega, *Shallow donor in semiconductor heterostructures: Fractal dimension approach and the variational principle*, Phys. Rev. B **67**, 115317 (2003)

I. D. Mikhailov, F. J. Betancur, R. A. Escorcia, and J. Sierra-Ortega, *Stability of D^- in quantum wells under strong magnetic fields*, Phys. Stat. Sol. (c) **0**, 747 (2003)

I. D. Mikhailov, F. J. Betancur, R. A. Escorcia, and J. Sierra-Ortega, *Off-Center Neutral and Negatively Charged Donor Impurities in Semiconductor Heterostructures: Fractal Dimension Method*, Phys. Stat. Sol. (b) **234**, 590 (2002)

I. D. Mikhailov, R. A. Escorcia, and J. Sierra-Ortega, *The Binding Energies of Shallow Donor Impurities in GaAs-(Ga, Al)As Coaxial Quantum-Well Wires*, Phys. Stat. Sol. (b) **220**, 195 (2000)

R. A. Escorcia, J. Sierra-Ortega, and R. Robayo, *Donor Binding Energy in Dielectric Graded GaAs-(Ga, Al)As Quantum-Well Wires*, Rev. Col. Fís. **34**, 645 (2002)

J. Sierra-Ortega, R. A. Escorcia, and S. T. Pérez-Merchancano, *Off-Center Donor Fractal Dimension in Graded Quantum-Well Wires* , Rev. Col. Fís. **33**, 144 (2001)